Modular and distinct PlexinA4/Farp2/Rac1 signaling controls dendrite morphogenesis

Victor Danelon[1#], Ron Goldner[2#], Edward Martinez[1], Irena Gokhman[2], Kimberly Wang[1], Avraham Yaron[2*], Tracy S. Tran[1*]

1. Department of Biological Sciences, Rutgers University, Newark, NJ 07102, USA
2. Department of Biomolecular Sciences, The Weizmann Institute of Science, Rehovot 76100, Israel

# Authors contributed equally to the study

* Corresponding Authors: Tracy S. Tran, tstran@rutgers.edu; Avraham Yaron, avraham.yaron@weizmann.ac.il

Lead contact: Tracy S. Tran, tstran@rutgers.edu

Running Title: The multifunctional guidance cue semaphorin 3A promotes dendritic arborization, but not axonal repulsion, through PlexinA4/Farp2/Rac1 signaling *in vitro* and *in vivo*.

Key words: Dendritic branching, axonal repulsion, Semaphorin, multifunctional guidance receptors, neural development

Number of pages: 45

Number of figures: 10

Number of words for abstract: 198

Number of words for introduction: 650

Number of words for discussion: 1195

Conflict of Interests: The authors declare that they have no conflict of interests.

Acknowledgements: The authors would like to thank Alex Kolodkin and Oren Schuldiner for providing critical feedback to this work. Also, we thank Adefemi Baderinwa and Michelle Davis for their excellent technical support with mouse genotyping. This work was support by NSF-IOS/BOI grant (1556968), and BSF grant (2013052) to T.S.T. and A.Y. Research in the lab of

T.S.T. is also supported by the NJ Governor's Council for Medical Research and Treatment of Autism (grant #CAUT17BSP022), the NJ Commission on Spinal Cord Research (grant #CSCR16IRG013), and Rutgers University – Newark Chancellor's Initiative for Multidisciplinary Research Teams Award. Research in the lab of A.Y. is supported by a research grant from the Jeanne and Joseph Nissim Center for Life Sciences Research at the Weizmann Institute of Science and the Nella and Leon Benoziyo Center for Neurological Diseases. A.Y. is an incumbent of the Jack and Simon Djanogly Professorial Chair in Biochemistry.

Abstract

Diverse neuronal populations with distinct cellular morphologies coordinate the complex function of the nervous system. Establishment of distinct neuronal morphologies critically depends on signaling pathways that control axonal and dendritic development. The Sema3A-Nrp1/PlxnA4 signaling pathway promotes cortical neuron basal dendrite arborization but also repels axons. However, the downstream signaling components underlying these disparate functions of Sema3A signaling are unclear. Using the novel *PlxnA4*$^{KRK\text{-}AAA}$ knock-in male and female mice, generated by CRISPR/cas9, we show here that the KRK motif in the PlxnA4 cytoplasmic domain is required for Sema3A-mediated cortical neuron dendritic elaboration but is dispensable for inhibitory axon guidance. The RhoGEF Farp2, which binds to the KRK motif, shows identical functional specificity as the KRK motif in the PlxnA4 receptor. We find that Sema3A activates the small GTPase Rac1, and that Rac1 activity is required for dendrite elaboration but not axon growth cone collapse. This work identifies a novel Sema3A-Nrp1/PlxnA4/Farp2/Rac1 signaling pathway that specifically controls dendritic morphogenesis but is dispensable for repulsive guidance events. Overall, our results demonstrate that the divergent signaling output from multifunctional receptor complexes critically depends on distinct signaling motifs highlighting the modular nature of guidance cue receptors and its potential to regulate diverse cellular responses.

Significance Statement

The proper formation of axonal and dendritic morphologies is crucial for the precise wiring of the nervous system that ultimately leads to the generation of complex functions in an organism. The Semaphorin3A-Neuropilin1/PlexinA4 signaling pathway has been shown to have multiple key roles in neurodevelopment, from axon repulsion to dendrite elaboration. This study demonstrates that 3 specific amino acids, the KRK motif within the PlexinA4 receptor cytoplasmic domain, are required to coordinate the downstream signaling molecules to promote Sema3A-mediated cortical neuron dendritic elaboration, but not inhibitory axon guidance. Our results unravel a novel Semaphorin3A-PlexinA4 downstream signaling pathway and shed light on how the disparate functions of axon guidance and dendritic morphogenesis are accomplished by the same extracellular ligand *in vivo*.

Introduction

The development of precise neuronal connections critically depends on proper extension of axons and elaboration of dendrites. Studies of neurite outgrowth and axon guidance are well established (Barnes and Polleux, 2009; Kolodkin and Tessier-Lavigne, 2011; Stoeckli, 2018), and while numerous studies were conducted in invertebrates (Jan and Jan, 2010), much less is known about the signaling mechanisms controlling dendritic morphogenesis in the mammalian nervous system. Interestingly, molecular cues initially described as axonal guidance cues also control later events in dendrite development, suggesting that these cues are multifunctional (Anzo et al., 2017; Mlechkovich et al., 2014; Nagel et al., 2015; Smith et al., 2012; Tran et al., 2009; Whitford et al., 2002; Yaron et al., 2005).

The Semaphorin family of multifunctional cues has been mainly studied in the context of axon guidance (Huber et al., 2003; Jin and Strittmatter, 1997; Tong et al., 2007; Toyofuku et al., 2005; Tran et al., 2007; Zanata et al., 2002). Semaphorins can repel or attract axons by engaging different co-receptors (Castellani et al., 2000; Chauvet et al., 2007) or interacting with molecules in the local environment (Kantor et al., 2004). Interestingly, the class 3 secreted Semaphorin-3A (Sema3A) can repel axons and promote dendrite branching in different neuronal populations both *in vitro* and *in vivo* (Fenstermaker et al., 2004; Gu et al., 2003; Mlechkovich et al., 2014; Tran et al., 2009; Yaron et al., 2005). However, the intracellular events orchestrating these divergent outputs, elicited by the same Sema3A cue, are largely elusive.

Sema3A signaling requires the binding to its obligate partner Neuropilin-1 (Nrp1) and formation of a complex with one of the Type-A Plexins (Plxns) (Tran et al., 2007). However, little was known about the specific Plxn signaling receptor involved in dendrite development until we showed the reduced dendritic complexity of *PlxnA4* knockout deep cortical neurons *in vivo* (Tran et al., 2009) that phenocopied those observed in the $Nrp1^{sema-}$ mutants (Gu et al., 2003). We demonstrated *in vitro* the ability of Sema3A to mediate growth cone collapse in dorsal root ganglion (DRG) neurons versus dendritic arborization of cortical neurons is embedded in a

modular nature of the PlxnA4 receptor, within its distinct cytoplasmic domains (Mlechkovich et al., 2014). We showed that the KRK motif in PlxnA4 can associate with the Rho-GEF Farp2 and is required for dendrite elaboration *in vitro*. However, the downstream signaling elements controlling dendrite elaboration versus axon guidance remained elusive.

Regulators of small GTPases - GEFs and GAPs - may represent signaling-specificity elements for divergent semaphorin functions. The RacGAP β2-Chimaerin is required for Sema3F induced axonal pruning but not repulsion (Riccomagno et al., 2012). The PlxnA2 GAP activity is required for proper distribution of dentate gyrus granule cells, but not for mossy fiber-CA3 targeting in the developing hippocampus (Zhao et al., 2018). These studies, along with our work, suggest that the Nrps/PlxnA complexes can recruit different GEFs and GAPs through distinct motifs, or the GAP domain itself, within the receptor to induce distinct cellular responses. Thus, we hypothesize that the KRK motif in PlxnA4 could serve as a recruitment site for specific GEFs, such as Farp2, to selectively confer Sema3A-dependent dendrite morphogenesis in cortical neurons *in vivo*.

Here, we generated a mouse line harboring an AAA substitution of the basic KRK motif in the PlxnA4 intracellular domain. Using this mouse line, we show that this conserved motif is required for Sema3A-induced dendritic elaboration in cortical neurons, but not for axonal repulsion or growth inhibition of several axonal tracts in the PNS and CNS. We demonstrated that cortical neuron dendrite development mediated by PlxnA4 signaling requires Farp2 *in vivo*. Furthermore, we show that Sema3A induces Rac1 activation in a Farp2-dependent manner in cortical neurons, and that this activity is selectively required for dendritic arborization, but not for growth cone collapse. Our work uncovers a distinct pathway for dendritic elaboration, specifically engaging the KRK motif of the multifunctional PlxnA4 receptor and its downstream signaling effectors.

Materials and Methods

Mouse strains

Mice harboring a point mutation in which the intracellular KRK (Lysine-Arginine-Lysine) motif of Plexin-A4 was replaced by a triplet of Alanines (*PlxnA4*$^{KRK>AAA}$) were generated by CRISPR/Cas9-based homologous recombination of a 164bp ssDNA oligonucleotide containing the KRK (5'-AAACGAAAA-3') to AAA (5'-GCAGCAGCA-3') mutation. A guide RNA (5'-CGCCATTGTCAGCATCGCGG-3') was designed to target exon 20 of *PlxnA4* with minimal off-target effects. The ssDNA oligonucleotide had 76-79bp homology arms around the KRK>AAA point mutation, with disruption of the TGG PAM sequence to TAG. *In vitro* transcribed Cas9 RNA (100 ng/µl), the sgRNA (50 ng/µl), together with the ssDNA (200 ng/µl), were injected into one cell fertilized embryos isolated from superovulated CB6F1 hybrid mice (F1 of BALB/cAnNHsd inbred female × C57BL/6NHsd inbred male) mated with CB6F1 males from Harlan Biotech Israel Ltd. (Rehovot, Israel). Injected embryos were transferred into the oviducts of pseudopregnant ICR females. Screening of tail tip DNAs was carried out by PCR genotyping and confirmed by sequencing. Heterozygous males were backcrossed with females of CD1(ICR) genetic background.

For generation of the *Farp2* KO mouse line, two CRISPR sgRNAs were designed flanking a 18,167bp sequence in the *Farp2* locus on Chr1 (GRCm38-mm10) including the promoter, the first utr exon and the second exon (with ATG). One sgRNA (5'-TCTTAAGGACTTATTGCCAA-3', chr1: 93511211-93511211) was targeted to a region upstream of the Farp2 gene promoter, and a second sgRNA (5'-GTGAGGGCCTCATTCCGAAA-3', chr1: 93529378-93529397) to intron 2. The sgRNAs were designed using several CRISPR designing tools, and optimized for the best guides, including: the MIT CRISPR design tool (Hsu et al., 2013) and sgRNA Designer, Rule Sets 1 and 2 (Doench et al., 2016; Doench et al., 2014), in both the original sites and later in the Benchling implementations (www.benchling.com), SSC (Xu et al., 2015), and sgRNA scorer (Chari et al., 2015), in their websites. *In vitro* transcribed Cas9 RNA (100 ng/µl) and the

sgRNAs (50 ng/µl) were injected into one cell fertilized embryos isolated from superovulated CB6F1 hybrid mice (F1 of BALB/cAnNHsd inbred female × C57BL/6NHsd inbred male) mated with CB6F1 males from Harlan Biotech Israel Ltd. (Rehovot, Israel). Injected embryos were transferred into the oviducts of pseudopregnant ICR females. Screening of tail tip DNAs was carried out by PCR genotyping and reverse transcription PCR (**Fig. 1**). Heterozygous males were backcrossed with females of CD1(ICR) genetic background.

To investigate the role of Farp2 in mediating Sema3A cortical dendritic-arborization we used *Farp2* KO mice generated by (Takegahara et al., 2010)**.** The following oligonucleotide primers were used to identify the rearranged *Farp2* locus: primer 1 (5-ATCAAACTCCACCCTGAGGTCCATG-3), primer 2 (5-TTTGTAAACTGCAGCGTTTCTCTTC-3), and primer 3 (5-CTTCTGAGGGGATCGGCAAT-3).

Mice harboring the Thy1-EGFP (M line) transgene were obtained at JAX (Jackson Laboratory, Bar Harbor, ME, USA; STOCK 007788 Tg-Thy1-EGFP-MJrs/J) and maintained by breeding with female C57BL/6J wild type mice. *PlxnA4* KO mice were previously described (Yaron et al., 2005). Embryonic day (E) 0.5 was considered to be the day a vaginal plug was found. Pups born were weaned at postnatal day (P) 21 and housed under a 12 h light/12 h dark cycle at constant temperature with food and water *ad libitum*. All animal work in this study has been approved by the Institutional Animal Care and Use Committees Rutgers University – Newark and The Weizmann Institute of Science.

Primary neuron cultures

For the growth cone collapse assay, DRGs from E13.5 embryos were dissected and plated as explants in chambers coated with 10µg/ml Poly-D-lysine (PDL, Sigma, cat. # P6407) and 10µg/ml Laminin (Sigma, cat. # L2020). Growing media was Neurobasal-A (Thermo Scientific, cat. # 10888-022) supplemented with 2% B-27 (Gibco, cat. # 17504044), 1% Penicillin-Streptomycin (Biological Industries, cat. # 03-031-1B), 1% L-Glutamine (Biological Industries,

cat. # 03-020-1B), and 25ng/ml NGF (Alomone, cat. # AN-240). After 48hrs, explants were treated with 0.1, 0.5, or 1nM AP-Sema3A for 30mins, then fixed with 4% Paraformaldehyde + 15% Sucrose solution, and stained with Phalloidin-Rhodamine (Sigma-Aldrich, cat. # P1951, 1:250) for visualization of F-actin filopodia. Growth cones with no or few filopodia were considered as collapsed. Percentage of collapsed growth cones was calculated for each treatment group and control.

For the collagen axonal repulsion assay, DRGs from E13.5 embryos were dissected and placed in droplets of 2mg/ml collagen (Roche, cat. # 11179179001) together with COS1 aggregates transfected with either secreted Myc-Sema3A or control PAY1-GFP. Co-cultures were grown for 48hrs in the aforementioned Neurobasal-A growth medium + 12.5ng/ml NGF, then fixed with 4% PFA and stained with anti-Tubulin βIII antibody (R&D systems, Tuj1 clone, 1:1000). Extent of axonal repulsion was measured by the ratio between the lengths of the proximal axons (i.e., axons that are close to the COS1 aggregate) to the length of the distal axons.

Cortical neurons were obtained from E13.5 wild-type, or from *PlxnA4* KO, *PlxnA4*$^{KRK\text{-}AAA}$ and *Farp2* KO mice as previously described (Mlechkovich et al., 2014). When the experiments required, dissociated neurons were transfected with Farp2-HA-tagged (Mlechkovich et al., 2014) using Amaxa™ Mouse Neuron Nucleofector™ Kit cat. # VPG-1001. The neurons were plated onto glass coverslips (coated with poly-D-lysine, 0.1mg/ml, cat. # P6407) in 12-well plates (TPP® 92412) and cultured with Neurobasal growth medium supplemented with 2% B-27 (cat. # 17504-044), 1% penicillin/streptomycin (cat. # 15140122), and 1% Glutamax (cat. # 35050) for 4-5 days.

Production of AP-Sema3A

Alkaline phosphatase (AP)-tagged Sema3A were produced in HEK293T cells as previously described (Mlechkovich et al., 2014). Briefly, HEK293T cells (ATCC cat. # CRL-3216,

RRID:CVCL_0063) were grown in Dulbecco's modified Eagle's medium (DMEM) supplemented with 10% fetal bovine serum (VWR, cat. # 97068-085) and 1% penicillin-streptomycin. The cells were transfected using BioT (cat. # B01-01) with an AP-Sema3A expression vector (Huber et al., 2005). The conditioned medium was concentrated using Amicon® ultra-15 UFC 910024 (Millipore). AP-Sema3A concentration was determined by AP activity assay (using AP substrate buffer para-nitrophenyl phosphate, Sigma) (Mlechkovich et al., 2014).

Rac1 activity assay

Rac1 activation was measured by using a Rac1 activation assay kit (Rac1 Pull-down Activation Assay Biochem Kit bead pull-down format, Cytoskeleton, Inc., cat. # BK035), following the manufacturer's protocol, with minor modifications. Briefly, fresh lysates of primary cortical neurons at DIV 5 incubated either with AP (5nM) or Sema3A-AP (5 nM) for 30 min were incubated with the glutathione S-transferase (GST)-fused p21-binding domain of Pak1 (GST-Pak1-PBD) at 4C for 1 h with gentle shanking and then the PAK-PBD beads were pelleted by centrifugation at 3-5,000 x g at 4°C for 1 min. After being washed once with Wash buffer, the beads were eluted in reduced 2x SDS sample buffer (Laemmli buffer) and analyzed by western blot. The Rac1 antibody used was anti-Rac1 (Abcam cat. # ab33186), concentration 0.6µg/ml.

Rac inhibitor EHT1864

For cortical neurons: EHT1864 (Tocris Bioscience, cat. # 3872, Batch # 1J/197009), inhibitor of Rac family GTPases (Onesto et al., 2008; Shutes et al., 2007), was prepared following manufacturer guidelines. Cortical neurons were incubated with EHT1864 at different concentrations (2.5, 5 and 10µM) (Gaitanos et al., 2016) for 2 hr at 37°C before treatment and also added with either 5nM of AP-Sema3A or AP alone treatment. DRG explants were incubated with the specified EHT1864 concentration for 30min at 37°C prior to Sema3A bath application. The same volume of H_2O was added to the no inhibitor treatment control cells.

Rac1 siRNA

The siRNA was purchased from Dharmacon™. Rac1 siRNA: cat. # M-041170-01-0005, siGenome Mouse Rac1 (19353) siRNA-SMART pol, 5nmol. Target sequences: D-041170-01 GGACGAAGCUUGAUCUUAG; D-041170-02 AGACGGAGCUGUUGGUAAA; D-041170-03 GAUCGGUGCUGUCAAAUAC; D-041170-04 GCAAAGUGGUAUCCUGAAG

Scrambled siRNA: cat. # D-001206-13-05, siGENOME Non-Targeting siRNA Pool #1, 5nmol. Target sequences: UAGCGACUAAACACAUCAA, UAAGGCUAUGAAGAGAUAC, AUGUAUUGGCCUGUAUUAG, AUGAACGUGAAUUGCUCAA. The Rac1 siRNA or the Scramble were transfected to cortical neurons using Amaxa^{TM} Mouse Neuron Nucleofector^{TM} Kit cat. # VPG-1001.

Immunohistochemistry

After 4-5 DIV, cortical neurons were treated with 5 nM AP-Sema3A or AP alone for 24 hours, fixed in 4% paraformaldehyde (PFA) at 4°C for 15min and processed for immunocytochemistry, as previously described (Mlechkovich et al., 2014). Primary antibodies used: monoclonal rabbit anti-MAP2 (1:1000, Cell Signaling Technology, 4542S), monoclonal mouse anti-HA (1:500, Santa Cruz Biotechnology F7 sc-7392). Secondary fluorescently conjugated antibodies were Alexa Fluor 488 donkey anti-mouse immunoglobulin G (IgG) (1:500, Jackson Immuno Research Laboratories), and Cy3 donkey anti-rabbit (1:1000, Jackson Immuno Research Laboratories). Coverslips were mounted on microscope slides using Mowiol (cat. # 81381 Aldrich)/ 10% p-Phenylenediamine (PPD, cat # 78460).

For cell surface expression of PlxnA4 and PlxnA4$^{KRK\text{-}AAA}$ protein, non-permeabilized primary cortical neurons were immunostained using 1:1000 Rabbit monoclonal Plexin-A4 (C5D1).

For whole-mount Neurofilament staining, embryos at E12.5 were collected into PBSx1, washed twice x5mins with PBSx1+0.2% Triton-x100 (PBST), and fixed with 4% PFA for 3hrs at room

temperature. Embryos were washed three times x10mins with PBST, dehydrated by incubation in increasing concentrations of Methanol in PBSx1 (10, 30, 50 and 80%, 1hr each), and stored overnight at 4°C in bleaching solution made of 6% H_2O_2 and 80% Methanol in PBSx1. Embryos were then washed three times x 1hr with 80% Methanol in PBSx1, rehydrated with decreasing Methanol concentrations in PBSx1 (50, 30 and 10%, 1hr each), washed three times x30mins with PBST and blocked overnight at 4°C with 2% milk powder + PBST (PBSMT). Following three days incubation with primary mouse anti-Neurofilament antibody (2H3, DSHB, 1:200 in PBSMT) at 4°C, embryos were washed six times with PBSMT x1hr and incubated overnight at 4°C with secondary HRP-coupled goat anti-mouse antibody (1:200) in PBSMT+2% goat serum. Embryos were washed four times with PBSMT+2% goat serum x1hr, then two times with PBST x1hr, and incubated for 30mins in 0.1M Tris pH7.5 + 3,3'-Diaminobenzidine tetrahydrochloride (DAB, Sigma-Aldrich, 1 tablet per 15ml) pre-filtered using a 0.45µm filter. Development was performed by addition of H_2O_2 to the DAB solution (0.03% H_2O_2 final concentration), and stopped with two PBSx1 washes x2mins, post-fixation with 4% PFA for 15mins, and additional three PBSx1 washes x5mins.

For whole-mount Tyrosine-Hydroxylase staining, embryos at E13.5 were collected and their sympathetic ganglia were exposed by dissection. Embryos were fixed with 4% PFA overnight at 4°C, washed with PBSx1 + 1% Tween-20 (PBST) x 10mins, and incubated for 2hrs in 0.9% NaCl made in PBSx1. Dehydration was carried out as described for the anti-Neurofilament staining (but 15mins each instead of 1hr), followed by bleaching in 6% H_2O_2 g + 20% DMSO in 80% Methanol in PBSx1. Embryos were rehydrated (15mins each), washed, blocked for 3hrs at room temperature with TBSx1 pH 7.4 + 1% Tween-20 (TBST) + 5% milk powder (TBSMT), then incubated for two days at 4°C in primary rabbit anti-Tyrosine-Hydroxylase antibody (Abcam, 1:200, in TBSMT + 5% DMSO). After 6 washes x1hr with TBST, embryos were incubated overnight at 4°C with secondary HRP-coupled goat anti-rabbit antibody (1:200) in TBST + 2%

goat serum, then washed five times x1hr with TBST, followed by 1hr wash with TBSx1. Development was performed as described for the anti-Neurofilament staining.

Golgi Staining

Adult (2-3 months old) mouse brains were processed for Golgi staining as previously described ((Tran et al., 2009); FD Rapid GolgiStain Kit, cat. # PK401, FD NeuroTechnologies) for 10 days. After incubation all brains were blocked and embedded in OCT embedding medium (Tissue-Tek, cat. # 4583). Sagittal sections (100 μm) were cut with a cryostat (Microm International, HM 505E) and mounted on charged microscopes slides (Diamond™ white glass). Staining procedures were followed exactly as described (FD NeuroTechnologies). Only layer 5 pyramidal neurons from the medial somatosensory cortex were included in our analyses. Differential interference contrast (DIC) z-stack images were taken with a Zeiss Axio Examiner Z1, Yokogawa spinning disc microscope.

Confocal images

High-resolution confocal z-stack images of MAP2- immunostained neurons were taken using a Zeiss Axio Examiner Z1, Yokogawa spinning disc microscope with an oil immersion 63× (NA 1.4) objective (PlanApo, Zeiss). High-resolution confocal z-stack images of GFP-positive cortical neurons from wild-type (WT) *Thy1-EGFP*, *PlxnA4*$^{KRK\text{-}AAA}$*; Thy1-EGFP* and *PlxnA4*$^{+/KRK\text{-}AAA}$*/Farp2* $^{+/-}$; *Thy1-EGFP* animals were taken using a LSM510 META Zeiss microscope. Series of optical sections were acquired in the z-axis at 1μm intervals through individual layer 5 pyramidal neurons. Maximum projections of fixed images were analyzed using FIJI (is just Image J) software.

Quantification of Dendritic arborization

Dendritic arborization was analyzed with the following parameters:

Sholl analysis. All Golgi-labeled z-stack images were reconstructed using FIJI and Adobe Photoshop CS6, and all analyses were performed using the Fiji Sholl Analysis plugin (Ferreira et al., 2014). For cortical basal dendrite Sholl analysis, the starting radius is 10 μm and the ending radius is 60 μm from the center of the neuron soma; the interval between consecutive radii is 5 μm (Mlechkovich et al., 2014).

Total dendritic length. The total dendritic length was measured using the ImageJ plugin NeuronJ (http://www.imagescience.org/meijering/software/neuronj/), calculated in microns (μm).

Dendritic complexity index (DCI). Dendritic order is defined as follows: primary dendrites were traced from the cell soma to the tip of the entire dendritic length, and secondary and tertiary dendrites were traced from the tip to the dendritic branch point using Adobe Photoshop software. Dendrite lengths that were less than 10μM of the cell soma were disregarded. The DCI was calculated using the following formula: (Σbranch tip orders + # branch tips)/(# primary dendrites) × (total arbor length) (Lom and Cohen-Cory, 1999; Peng and Tran, 2017).

For each parameter analyzed, at least 30-40 neurons, from 3-4 independent cultures/mice, per condition measured.

Western blot

For Figure 1, panels B-C: tissues were lysed with radio immunoprecipitation assay (RIPA) buffer (50mM Tris pH 7.4, 159mM NaCl, 1% NP40, 0.1% SDS, 0.5% Deoxycholate, 1mM EDTA in ddH_2O) supplemented with 1:25 cOmplete™ Protease Inhibitor Cocktail (Roche, cat. # 11697498001) and 1:200 PMSF. Samples then underwent two cycles of 10mins long incubation on ice followed by 10secs of vortexing. After 14,000g centrifugation for 15mins at 4°C, supernatant was collected and protein concentration was measured using Pierce™ BCA Protein Assay Kit (Thermo Scientific, cat. # 23227) and Gen5 3.04 software (BioTek). Sample buffer X5 (125 mM Tris HCl pH 6.8, 25% β-mercaptoethanol, 43.5% glycerol, 10% SDS, 0.05% bromophenol blue) was added to the samples that were further denatured by boiling at 95°C for

5mins. Samples were separated by SDS-PAGE and electrophoretically transferred onto nitrocellulose membranes. Non-specific antigen sites were blocked using 5% milk in TBS (10 mM Tris pH 8, 150 mM NaCl) and 0.1% Tween-20 (TBST) for 1hr at room temperature. Antigen detection was performed by overnight incubation with appropriate antibodies: 1:1000 Rabbit monoclonal Plexin-A4 (cat. # C5D1) anti-mouse (Cell Signaling, cat. # 3816), 1:1000 Rabbit monoclonal Neuropilin-1 (cat. # D62C6) anti-mouse (Cell Signaling, cat. # 3725), 1:30,000 mouse anti-Actin antibody C4 (MP Biomedicals, cat. # 08691001). Antibodies were diluted in 5% BSA in TBST +0.05% Sodium azide. Membranes were then washed and incubated for 1hr in at room temperature in Goat anti-Rabbit HRP (JIR – Jackson Immuno-Research Laboratory, 111-035-003) or Goat anti-Mouse (JIR – Jackson Immuno-Research Laboratory, 115-035-003) secondary antibodies, following incubation in WesternBright™ HRP-substrate ECL (Advansta, cat. # K-12045-D20) and exposure to Super RX-N X-Ray films (Fujifilm, cat. # 47410). Films were scanned and band intensities were quantified using Image J (Fiji) software.

For Figure 1, panel D: Mice were sacrificed using a CO_2-chamber. The cortices were immediately removed from the skull and homogenized in RIPA buffer containing protease inhibitors (Roche cOmplete® Ref. 11697498001). Homogenates were cleared by centrifugation at 500 g twice for 7 min and protein concentration was determined using the Bradford protocol (Bradford, 1976); samples were then boiled in gel-loading buffer and separated using sodium dodecyl sulfate-polyacrylamide gel electrophoresis (SDS-PAGE,) 10% for PlxnA4 (cat. # C5D1, Cell signaling Technology), and IgG. Proteins were transferred to nitrocellulose membranes (cat. # 1620097 Bio-Rad Laboratories Inc., PA, USA) and blocked with 5% non-fat milk in Tris-buffered saline with 0.05% Tween, for 1hr at room temperature. The membranes were incubated with primary antibodies (overnight at 4°C), washed, and reincubated with the secondary HRP conjugated antibody (1:2000 dilution for anti-rabbit -GE Healthcare, NA934, Lot. 6969611; 1:2000 anti-mouse -GENXA931; 1 hr at room temperature). Peroxidase activity was visualized by using enhanced chemiluminescence (ECL) kit (cat. # 32106, Thermo Fisher

Scientific). ECL signal was exposed to BioBlue Lite® films XR8813. Membranes were re-probed with a monoclonal antibody against IgG for control of protein loading. The images were quantified using the FIJI software.

Co-immunoprecipitation assay

Mice were sacrificed using a CO_2-chamber and the cortices were immediately removed from the skull and homogenized in RIPA-modified buffer (TBS 1x, Glycerol 10%, Triton-X100 1% and NP40 1%) supplemented with protease inhibitors. Briefly, the homogenates were centrifuged at 14,000 × g for 10min, and 500µg of total protein from the supernatants was pre-cleared with Protein G Sepharose® 4 Fast Flow (GE Healthcare cat. # GE17-0618-01) for 2hr at 4°C. After centrifugation, the pre-cleared supernatants were incubated with anti-Nrp1 (R&D System, cat. # AF566) at 4°C for overnight. Then 10 µl protein Protein G Sepharose® 4 Fast Flow were added, incubated at 4°C for 4hr. The immunoprecipitates were washed with ice-cold RIPA-modified buffer, eluted with SDS sample buffer, and analyzed by WB. Membranes where then probed with anti-PlxnA4 (cat. # C5D1, Cell signaling Technology) antibody. As a protein loading control, we first incubated the membranes with the secondary antibody anti-goat alone (primary antibody from goat).

Cell-surface biotinylation assay

Cortical neurons from E13.5 embryos were extracted and grown in culture. At 7DIV, a cell surface biotinylation assay was performed using a commercially available kit (Pierce Cell Surface Protein Isolation Kit, Thermo Scientific, cat. # 89881). Eluates were subjected to immuno-blot analysis using a Plexin-A4 antibody (Cell Signaling, cat. # 3816), as described above in the western blot method details. Cell lysates obtained following the biotinylation process were used as loading controls, and the total mass of proteins between ~120-260kDa was used for quantification and normalization purposes.

Reverse Transcription Quantitative Real-Time PCR

Heads of E13.5 embryos were collected and subjected to RNA extraction. Briefly, heads were homogenized in TRI reagent® (Sigma) and chloroform was added. Samples were mixed thoroughly, incubated at room temperature for 10mins, centrifuged at 13,000RPM for 15mins at 4°C, and upper RNA-containing phase was collected. Precipitation of RNA was performed using Isopropanol, after which samples were incubated at room temperature for 10mins, and centrifuged at 13,000RPM for 15mins at 4°C. Cold 75% Ethanol was added to the RNA pellet, and samples were stored overnight at -80°C. The next day, Ethanol was decanted and samples were incubated at 65°C for 5mins to remove all traces of Ethanol. RNA pellet was liquidized with 30µl ultrapure DNase/RNase free H_2O, and RNA concentration was measured using NanoDrop spectrophotometer. cDNA was then synthesized from 1µl/RNA sample using an iScript kit (Bio-Rad, cat. # 1708891), and *PlxnA4* expression levels were measured by quantitative real-time PCR reaction using KAPA SYBR® FAST ABI prism® qPCR kit (KAPABIOSYSTEMS, cat. # KK4605). Primers (5'-3') were: *PlxnA4* – GCAAGAACTTGATCCCGCCT and GTCACGGTGCATGGTTTCTC; *Actb* – GGCTGTATTCCCCTCCATCG and CCAGTTGGTAACAATGCCATGT. Results were subjected to relative quantification analysis (ΔΔCt) using Microsoft Excel software.

Experimental Design and Statistical Analyses

For sequencing analysis of exon 20 in the *PlxnA4* locus experiments, a total of 3 animals were used. For PlxnA4 mRNA RT-qPCR analysis, a total of 6 animals/genotype were used and a Student's t-test was performed. For western blot analysis of PlexinA4, Neuropilin1 and actin proteins in E13.5 DRGs and cortices extracted from $PlxnA4^{KRK\text{-}AAA}$, WT littermate and *PlxnA4* KO, a total of 4 mice/genotype were used from 3 independent experiments. For western blot analysis of Neuropilin1:PlexinA4 interaction, cerebral cortices were extracted from $PlxnA4^{KRK\text{-}}$

^{AAA}, WT littermate and *PlxnA4* KO, a total of 3 animals/genotype were used from 3 independent experiments. For analysis of the expression pattern of the PlxnA4 protein, primary cortical neurons obtained from WT, *PlxnA4*$^{KRK\text{-}AAA}$ and *PlxnA4* KO embryos, were immuno-stained using a PlexinA4 antibody and a total of 3 independent cultures/genotypes. For analysis of PlexinA4's cell-surface expression level, 3 independent cell-surface biotinylation experiments were conducted and followed by an immuno-blot analysis using a PlexinA4 antibody. For the analysis of Sema3A-mediated growth cone collapse using DRG explants obtained from WT, *PlxnA4*$^{KRK\text{-}AAA}$ and *Farp2* KO embryos, a total of at least 300 growth cones/group from 3 independent experiments were analyzed and two-way ANOVA with post hoc Tukey test was performed. For the Sema3A-collagen axonal repulsion assay using DRG explants obtained from WT, *PlxnA4*$^{KRK\text{-}AAA}$ and *Farp2* KO embryos, a total of at least 8 DRGs/genotype from 3 independent experiments were used, and a Student's t-test was performed. For Sema3A-treatment in primary cortical neuron culture obtained from WT, *PlxnA4* KO, *PlxnA4*$^{KRK\text{-}AAA}$ and *Farp2* KO, a total of 3 independent cultures/genotype were used and a Student's t-test and a two-way ANOVA followed by post hoc Tukey test was performed. For Golgi-stained layer V cortical neurons obtained from Wild-Type, *PlxnA4* KO, *PlxnA4*$^{KRK\text{-}AAA}$, *Farp2* KO and *PlxnA4*$^{+/KRK\text{-}AAA}$ /*Farp2* $^{+/-}$, a total of 3 animals/genotype were used. For analysis of layer V cortical neurons in Wild-Type, *PlxnA4*$^{KRK\text{-}AAA}$ and in *PlxnA4*$^{+/KRK\text{-}AAA}$ /*Farp2*$^{+/-}$, using Thy1GFP mice, a total of 3 animals/genotype were used. For quantification of dendritic morphologies using Sholl analysis, dendritic length, DCI and number of dendritic tips one-way ANOVA and post hoc Tukey test was performed. For the analysis of the pattern of cutaneous sensory axons projections in WT, *PlxnA4*$^{KRK\text{-}AAA}$, *Farp2* KO or *PlxnA4* KO E12.5 embryos, using a Neurofilament antibody, a total of at least 8 embryos/genotype from at least 3 independent experiments were used. For the analysis of sympathetic axons projections in WT, *PlxnA4*$^{KRK\text{-}AAA}$, *Farp2* KO or *PlxnA4* KO E13.5 embryos, a total of at least 10 embryos/genotype from at least 3 independent experiments were used. For the analysis of the anterior commissure in WT, *PlxnA4*$^{KRK\text{-}AAA}$, *Farp2* KO or *PlxnA4*

KO, using hematoxylin staining, a total of at least 7 brains/genotype from at least 3 independent experiments were used. For the analysis of the Rac signaling in Sema3A-dependent growth cone collapse of Phalloidin-Rhodamine stained DRG neurons obtained from WT and *PlxnA4*$^{KRK-AAA}$ DRGs, a total of at least 300 growth cones/group from 3 independent experiments were analyzed and a two-way ANOVA with post hoc Tukey test was performed. For the analysis of the Rac signaling inhibition (using EHT) in Sema3A-dependent dendritic growth in WT cortical primary neurons, a total of 3 independent cultures were used and a two-way ANOVA followed by post hoc Tukey test was performed. For the analysis of Sema3A-dependent dendritic arborization in the Farp2 GEF knockout with Rac inhibitor, 3 independent cultures were performed, and a two-way ANOVA followed by post hoc Tukey test was performed. For the western blot of Rac1 knockdown experiments, using a specific Rac1 siRNA, 3 independent primary WT neuron cultures were used, and a Student's t-test was performed. For Sema3A treatment in the Rac1 knockdown experiments, a total of 3 independent primary WT cortical neuron cultures were used and two-way ANOVA followed by post hoc Tukey test. For the Pull-down assay showing the effect of 30min stimulation of Sema3A on Rac1 activation, 3 independent WT, *PlxnA4*$^{KRK-AAA}$ and *Farp2* KO primary neuron cultures were used and Student's t-test and one-way ANOVA was performed. For DRG growth cone collapse and cortical neurons dendritic arborization quantifications, data obtained were analyzed using GraphPad Prism Software. For DRG axonal repulsion, data were analyzed using Microsoft Excel software. Data are shown as mean ± SEM.

Results

Generation of the *PlxnA4*$^{KRK-AAA}$ mutant and *Farp2* knockout mouse

To explore the role of the KRK motif in the PlxnA4 cytoplasmic domain we have generated by CRISPR the *PlxnA4*$^{KRK-AAA}$ line that harbors a KRK substitution to AAA in the endogenous PlxnA4 receptor. The modified genomic area (220bp) from tail genomic DNA was sequenced

and only the desired modification was detected. The mutation had no effect on PlxnA4 mRNA or total protein levels, as shown using biochemical analysis (**Fig. 1A and 1B-C, respectively**). Moreover, we have not detected any change in the levels of the PlxnA4 co-receptor Neuropilin-1 (Nrp1, **Fig. 1B-C**), nor change in the association of Nrp1 with PlxnA4 in the *PlxnA4*$^{KRK\text{-}AAA}$ mutants (**Fig. 1D**). Furthermore, the KRK to AAA substitution did not affect the cell surface expression of PlxnA4 proteins on cortical neurons by detecting the biotinylated receptor (**Fig. 1E-F**) and its dendritic localization (**Fig. 1G**). Overall, our analysis shows that the KRK to AAA mutation is not affecting the expression and cellular distribution of Plexin-A4. In parallel, we have generated a *Farp2* KO mouse by CRISPR (**Fig. 1H**). Using PCR analysis of tail genomic DNA and reverse transcription analysis of progenies from the *Farp2* KO line, we also demonstrated successful deletion of the *Farp2* locus and its transcripts (**Fig. 1I-J**). For both mutant lines, the injected animals (F0) were crossed with wild-type (WT) CD1 mice three times. In all the experiments described below, WT littermate controls were used.

DRG sensory axons from *PlxnA4*$^{KRK\text{-}AAA}$ and *Farp2* knockout animals are sensitive to Sema3A inhibition and repulsion

The *PlxnA4*$^{KRK\text{-}AAA}$ and the *Farp2* mutant animals allowed us to systemically examine their role in Sema3A signaling using multiple *in vitro* assays. We first assessed the acute growth cone collapse assay. DRG axonal growth cones from E13.5 *PlxnA4*$^{KRK\text{-}AAA}$ homozygous mutant, grown for 2DIV and visualized with Phalloidin-Rhodamine, were able to respond to Sema3A-mediated collapse in a dosage dependent manner, similar to the WT control (**Fig. 2A-E**). In line with our results from the *PlxnA4*$^{KRK\text{-}AAA}$ mutant neurons, DRG axonal growth cones from mice deficient of Farp2 GEF (*Farp2* KO), which is a downstream target of the KRK motif in PlxnA4, collapsed at comparable percentages to the WT control following Sema3A treatment (**Fig. 2F-H**). Next, we tested the response to the prolonged Sema3A-mediated axonal repulsion in *PlxnA4*$^{KRK\text{-}AAA}$ and *Farp2* mutant animals. For this we co-cultured DRG explants with COS1 cell

aggregates either transfected with GFP (control) or a construct expressing Sema3A. Both DRG sensory axons from *PlxnA4*$^{KRK\text{-}AAA}$ and *Farp2* KO explants were repelled from the Sema3A source, similar to WT DRG axons (**Fig. 2I-M**). Quantification of axonal repulsion using the proximal/distal axonal outgrowth ratio measurement as previously described (Yaron et al., 2005) showed no significant difference between *PlxnA4*$^{KRK\text{-}AAA}$ or *Farp2* KO explants in comparison to their respective littermate WT controls in response to Sema3A repulsion (**Fig. 2N**; p=0.48). These results suggest that the KRK motif in the PlxnA4 receptor and its downstream target Farp2 are dispensable for both Sema3A-mediated acute growth cone collapse and prolonged axonal repulsion.

Cortical Neurons from *PlxnA4*$^{KRK\text{-}AAA}$ and *Farp2* knockout animals are non-responsive to Sema3A-induced dendrite elaboration

As *Sema3A* KO brains have previously been shown to display similar cortical neuron basal dendrite morphological defects (Nakamura et al., 2017) similar to those observed in *PlxnA4* KO (Mlechkovich et al., 2014; Peng and Tran, 2017; Tran et al., 2009), we asked whether the KRK motif of PlxnA4 and its downstream target Farp2 are required for Sema3A-mediated cortical dendrite branching. Embryonic cortical neurons at E13.5 were dissociated from WT, *PlxnA4*$^{KRK\text{-}AAA}$ mutant, *PlxnA4* KO and *Farp2* KO animals as previously described (Mlechkovich et al., 2014; Peng and Tran, 2017; Tran et al., 2009) and grown for 5 days *in vitro* (DIV) followed by Sema3A treatment for 24 hours and fixation for anti-MAP2 immunocytochemistry to visualize all dendrites (**Fig. 3A**). Using four different measurements, we quantified the number of dendritic intersections (by Sholl analysis, **Fig. 3B**), the total dendritic length (**Fig. 3C**), the dendritic complexity index (DCI, **Fig. 3D**) and the average number of dendritic tips (**Fig. 3E**). Consistent with previous results, Sema3A-treated WT neurons showed increased number of dendrites compared to the control-treated (Student t-test, **Sholl**: 10µm: t=4.775, p=0.0088; 15µm: t=5.422, p=0.0056; 20µm: t=5.706, p=0.0047; 25µm: t=5.119, p=0.0069, 30µm: t=4.443, p=0.0113;

35µm: t=4.458, *p*=0.0112; 40 µm: t=3.999, *p*=0.0161; 45µm: t=3.934, *p*=0.0170 ; 50µm: t=3.807, *p*=0.0190; 55µm: t=2.952, *p*=0.0419; 60µm: t=2.910, *p*=0.0437; **Length**: t=5.022, *p*=0.0074; **DCI**: t=7.175, *p*=0.0020; **Dendritic tips**: t=6.553, *p*=0.0028). Next, we asked whether neurons obtained from *PlxnA4*$^{KRK\text{-}AAA}$*, Farp2* KO and *PlxnA4* KO showed sensitivity to Sema3A treatment. We found that *PlxnA4*$^{KRK\text{-}AAA}$ mutant and *Farp2* KO neurons were insensitive to Sema3A stimulation, similarly to the *PlxnA4* KO (two-way ANOVA: **Sholl:** 10 µm: *p*=0.0023, F=7.554; 15 µm: *p*<0.0001, F=14.41; 20 µm: *p*<0.0001, F=18.04; 25 µm: *p*<0.0001, F=15.59; 30 µm: *p*=0.0002, F=12.09; 35 µm: *p*=0.0001, F=13.05; 40 µm: *p*=0.0004, F=10.59; 45 µm: *p*=0.0004, F=10.72; 50 µm: *p*=0.0015, F=8.284; 55 µm: *p*=0.0422, F=3.437; **Length**: *p*=0.0001, F=13,64; **DCI**: *p*<0.0001, F=27; **Dendritic tips:** *p*<0.0001, F=25.50). Similarly, there were no significant differences in dendritic morphology as measured by Sholl analysis, dendritic length, DCI and average number of dendritic tips between AP-treated WT neurons versus AP or Sema3A-treated *PlxnA4*$^{KRK\text{-}AAA}$ mutant, *PlxnA4* KO and *Farp2* KO neurons. In addition, we tested whether higher Sema3A concentration could induce dendrite growth in *PlxnA4*$^{KRK\text{-}AAA}$ mutant and *Farp2* KO neurons. *PlxnA4*$^{KRK\text{-}AAA}$ and *Farp2* KO cortical neurons were treated with 10nM of Sema3A for 24 hours. We analyzed the dendritic morphology measured by Sholl analysis, dendritic length, DCI and dendritic tips. We found that both *PlxnA4*$^{KRK\text{-}AAA}$ and *Farp2* KO cortical neurons remained non-responsive even to the higher concentrations of Sema3A treated for 24 hours (two-way ANOVA, **Sholl:** 10 µm: *p*=0.0075, F=7.565; 15 µm: *p*=0.0002, F=19.6; 20 µm: *p*<0.0001, F=22.55; 25 µm: *p*=0.0001, F=20.66; 30 µm: *p*=0.0005, F=15.11; 35 µm: *p*=0.0006, F=14.54; 40 µm: *p*=0.0018, F=11.25; 45 µm: *p*=0.0016, F=11.49; 50 µm: *p*=0.0025, F=10.30; 55 µm: *p*=0.0085, F=7.27; 60 µm: *p*=0.0132;, F=6.342; **Length**: *p*=0.0007, F=13.92; **DCI**: *p*< 0.0001, F=28.55; **Dendritic tips:** *p*=0.0002, F=18.58) (**Fig.4**). Therefore, in contrast to DRG sensory neurons, these results suggest that *PlxnA4*$^{KRK\text{-}AAA}$ mutant and *Farp2* KO cortical neurons are selectively non-responsive to Sema3A-mediated dendrite elaboration.

PlxnA4$^{KRK\text{-}AAA}$ and _Farp2_ knockout animals exhibit reduced basal dendritic arborization in layer 5 cortical neurons, but not axonal repulsion defects _in vivo_.

Next, we asked whether _PlxnA4_$^{KRK\text{-}AAA}$ homozygous mutant and _Farp2_ KO embryos display dendritic elaboration phenotypes in layer 5 pyramidal neurons _in vivo_. We performed Golgi staining to uniformly label all dendritic processes in adult brains of WT, _PlxnA4_$^{KRK\text{-}AAA}$ mutant, _PlxnA4_ KO and _Farp2_ KO animals. We observed severe reduction in the basal dendritic arbors of layer 5 cortical neurons in the _PlxnA4_$^{KRK\text{-}AAA}$ mutant, _PlxnA4_ KO and _Farp2_ KO brains compared to the WT (**Fig. 5A**). As revealed by Sholl analysis, there was a significant decrease in dendritic intersections between WT and _PlxnA4_$^{KRK\text{-}AAA}$ mutant or _PlxnA4_ KO or _Farp2_ KO (**Fig. 5B**; **Sholl:** 15µm: p<0.0001, F=50.83; 20µm: p<0.0001, F=32.55; 25µm: p< 0.0001, F=23.39; 30µm: p=0.0001, F=18.50; 35µm: p<0.0001, F=20.56; 40µm: p=0.0006, F=13.08; 45µm: p=0.0017, F=10.16; 50µm: p=0.0014, F=10.67; 55µm: p<0.0003, F=15.59; 60µm: p=0.0009, F=11.79). In addition, the total dendritic length, the dendritic complexity index (DCI) and average number of dendritic tips for _PlxnA4_$^{KRK\text{-}AAA}$ mutant, _PlxnA4_ KO and _Farp2_ KO were lower compared to WT (**Fig. 5C-E**; **Length:** p<0.0001, F=20.14; **DCI:** p=0.0005, F=13.81; **Dendritic tips:** p<0.0001; F=21.94). To provide genetic evidence that Farp2 is indeed downstream of PlxnA4 signaling, we generated compound heterozygous animals, _PlxnA4_$^{KRK\text{-}AAA/+}$; _Farp2_$^{+/-}$. The trans-heterozygous animals also exhibit reduced basal dendritic arbors, phenocopying the _PlxnA4_ KO (**Fig. 5A-E**; Sholl analysis between WT and _PlxnA4_$^{KRK\text{-}AAA/+}$;_Farp2_$^{+/-}$ and _PlxnA4_ KO; **Sholl:** 15µm: p=0.0011, F=15.93; 20µm: p<0.0001, F=38.17; 25µm: p=0.0002, F=25.58; 30µm: p=0.0004, F=20.52; 35µm: p=0.0003, F=23.31; 40µm: p=0.0011, F=16.07; 45µm: p=0.0023, F=12.83; 50µm: p=0.0016, F=14.43; 55µm: p=0.0002, F=25.78; 60µm: p=0.0015, F=14.63; **Length:** p=0.0002; F=25.71**; DCI:** p=0.0005; F= 19.45 **; Dendritic tips:** p=0.0003; F=23.90). In addition, we compared the number of dendritic intersections, dendritic length, DCI and number of dendritic tips between WT and _PlxnA4_$^{KRK\text{-}AAA/+}$ or _Farp2_$^{+/-}$ single heterozygous animals. There was not a significant difference between WT and

PlxnA4$^{KRK\text{-}AAA/+}$ or *Farp2*$^{+/-}$ heterozygous animals (images not shown), in contrast, there were significant differences between *PlxnA4*$^{+/KRK\text{-}AAA}$ single heterozygous or *Farp2*$^{+/-}$ single heterozygous and *PlxnA4*$^{KRK\text{-}AAA}$ mutant or *PlxnA4* KO or *Farp2* KO or compound heterozygous animals *PlxnA4*$^{KRK\text{-}AAA/+}$;*Farp2*$^{+/-}$ (Compared to *PlxnA4*$^{+/KRK\text{-}AAA}$ **Sholl:** 15µm: p=0.0156, F=4.601; 20µm: p=0.0002, F=13.32 ; 25µm: p<0.0001, F=18 ; 30µm: p<0.0001, F=24.58 ; 35µm: p=0.0001, F=14.49; 40µm: p=0.0013 , F=8.544 ; 45µm: p=0.0033, F=6.923; 50µm: p=0.0027, F=7.251; 55µm: p=0.0009, F=9.292; 60µm: p=0.0021 , F=7.641; **Length:** p<0.0001; F=20.18; **DCI:** p<0.0001; F=28.21**; Dendritic Tips:** p<0.0001; F=23.37 ; Compared to *Farp2*$^{+/-}$ **Sholl:** 15µm: p=0.008, F=5.531; 20µm: p=0.0001, F=13.87; 25µm: p<0.0001, F=15.45; 30µm: p<0.0001, F=18.43 ; 35µm: p=0.0004, F=10.96; 40µm: p=0.0039, F=6.625; 45µm: p=0.0065, F=5.822; 50µm: p=0.0073, F=5.652; 55µm: p=0.0069, F=5.748; 60µm: p=0.0289; F=3.819; **Length**: p<0.0001; F=16.53; **DCI:** p<0.0001;F=37.28; **Dendritic Tips:** p<0.0001; F=20.32).

While the Golgi staining is a great method for assessing overall neuronal morphologies, the impregnation of the silver nitrate is arbitrary for each neuron. Therefore, to confirm that indeed layer 5 neuron basal dendrites are exhibiting the reduced dendritic arbor phenotype observed, we crossed the *PlxnA4*$^{KRK\text{-}AAA}$ mutant or the *Farp2* KO with Thy1-EGFP reporter mice to genetically label layer 5 neurons. We used the M line of Thy1-EGFP to sparsely label specific layer 5 neurons for optimal visualization of the entire dendritic arbor of each neuron. Consistent with our Golgi staining analysis, we found that *PlxnA4*$^{KRK\text{-}AAA}$ mutant;Thy1-EGFP+ and *PlxnA4*$^{KRK\text{-}AAA/+}$*;Farp2*$^{+/-}$;Thy1-EGFP+ (trans-heterozygous) neurons displayed significantly reduced basal dendritic arbors compared to WT Thy1-EGFP+ neurons (**Fig. 5F-G**, **Sholl:** 15µm: p<0.0025, F=13.94; 20µm: p<0.0076, F=9.531; 25µm: p<0.0031, F=12.99; 30µm: p<0.0006, F=21.14; 35µm p<0.0007, F=20.72; 40µm: p=0.0045, F=11.44; 45µm: p=0.0177, F=6.968).

In contrast to dendritic development, both *PlxnA4*$^{KRK\text{-}AAA}$ mutant and *Farp2* KO embryos at E12.5 showed normal sensory cutaneous axon patterning in the PNS, comparable to the WT, as opposed to the defasciculated, highly branched and misguided axonal projections seen in the

PlxnA4 null (**Fig. 6A-D**, arrows). Furthermore, it is well established that Sema3A-PlxnA4 signaling can exert axonal repulsion on different neuronal populations in both the PNS and CNS (Gu et al., 2003; Huber et al., 2005; Yaron et al., 2005). Besides repelling peripheral DRG axons, PlxnA4 is also required in the PNS for the proper projections of sympathetic axons, and for the formation of the anterior commissure in the CNS (Waimey et al., 2008; Yaron et al., 2005). Therefore, we asked whether the KRK motif in the PlxnA4 receptor is dispensable only for PNS DRG axon repulsion or can this be a general principal for Sema3A signaling in axon guidance. Tyrosine hydroxylase staining of the sympathetic ganglia showed normal axonal patterns in *PlxnA4*$^{KRK\text{-}AAA}$ mutant and *Farp2* KO E13.5 embryos similar to WT control, while *PlxnA4* KO animals displayed disorganized axonal projections towards the midline (**Fig. 6E-H**). Haematoxylin staining of coronal sections from WT, *PlxnA4*$^{KRK\text{-}AAA}$**,** *PlxnA4* KO and *Farp2* KO brains at P30 showed normal anterior commissure projections in both *PlxnA4*$^{KRK\text{-}AAA}$ mutant and *Farp2* KO animals, similar to the WT, but in contrast to the missing commissure in the *PlxnA4* KO mutant (**Fig. 6I-L**).

Taken together, these results suggest that the PlxnA4^{KRK}-Farp2 signaling pathway is necessary to promote layer 5 pyramidal neuron basal dendrite elaboration but is dispensable for axonal repulsion *in vitro* and *in vivo*.

Inhibition of Rac activity perturbs Sema3A-mediated cortical neuron dendrite elaboration, but not axon growth cone collapse

One of the major targets of Farp2 GEF is the small GTPase Rac1, but not other members of the Rho GTPase family – CDC42 or RhoA (He et al. 2013; Kubo et al. 2002; Toyofuku et al., 2005). A previous study showed that overexpression of Farp2 in murine primary neurons induced shortened neurites (Kubo et al., 2002), however, the physiological importance of Farp2-Rac1 signaling pathway in the nervous system is not clear. Therefore, we first asked whether Rac activation is required downstream of Sema3A-signaling for axonal growth cone collapse and

dendrite morphogenesis using a pharmacological approach. We used a validated pan-Rac GTPase inhibitor, EHT1864 (Onesto et al., 2008; Shutes et al., 2007), in a dosage-dependent manner on cultured WT DRG neurons and found that this inhibitor had no effect on Sema3A-induced growth cone collapse (**Fig. 7A-N**). However, WT dissociated cortical neurons treated with the Rac inhibitor for 2 hours before Sema3A stimulation, at concentrations of 2.5, 5 or 10µM, showed complete inhibition of dendritic elaboration, compared to Sema3A treated neurons without the inhibitor. In contrast, there were no significant differences in dendritic morphology between AP-treated WT neurons versus AP-treated+EHT at different concentrations (2.5, 5 and 10µM) (**Fig. 7O**). Quantifications of dendritic intersections by Sholl analysis (**Fig. 7P**), total dendritic length (**Fig. 7Q**), DCI (**Fig. 7R**) and average number of dendritic tips (**Fig. 7S**) showed significant differences between WT neurons treated with Sema3A only compared with Sema3A+2.5µM EHT, Sema3A+5µM EHT, Sema3A+10µM EHT, 2.5, 5 or 10µM EHT alone or control (no Sema3A, no EHT) (two-way ANOVA **Sholl:** 15µm: p=0.0019, F=7.822; 20µm: p=0.0012, F=8.652; 25µm: p=0.0005, F=10.19, 30µm: p=0.0020, F=7.798.117; 35µm**:** p=0.0019, F=7.895; 40µm**:** p=0.0181 F=4.492**; Length:** p=0.0276, F=3.674; **DCI:** p=0.0030, F=9.454; **Dendritic tips:** p=0.0013, F=7.381). These results establish that Rac activation is required for Sema3A-mediated dendrite outgrowth and branching.

Sema3A-mediated cortical neuron dendrite elaboration requires Rac1 activation by Farp2 GEF

To support our hypothesis that Sema3A-mediated dendrite elaboration involves a Farp2-Rac signaling pathway, we used *Farp2* KO cortical neurons, which we showed are insensitive to Sema3A-induced dendritic elaboration (**Fig. 3**). First, we demonstrate that by overexpressing Farp2 cDNA into *Farp2* KO neurons, the sensitivity to Sema3A-induced dendritic elaboration is restored compared to *Farp2* KO neurons transfected with Farp2 cDNA without Sema3A

treatment (**Fig. 8A-B**, two-way ANOVA **Sholl**: 10µm: *p*=0.0081, F=12.24; 15µm**:** *p*=0.0011, F=24.47; 20µm: *p*=0.0007, F=27.95; 25µm**:** *p*=0.0008, F=26.81, 30µm**:** *p*=0.0086, F=11.93). However, *Farp2* KO neurons were unable to elaborate dendrites when transfected with Farp2 cDNA + 2.5µM EHT and treated with Sema3A. Sholl analysis showed that the number of dendritic intersections significantly decreased between 10-30µm away from the cell soma in *Farp2* KO neurons rescued with Farp2 cDNA and treated with Sema3A+EHT compared to *Farp2* KO rescued with Farp2 cDNA and treated with Sema3A only (**Fig. 8A-B**; two-way ANOVA **Sholl**: 10µm: *p*=0.0132, F=10.05; 15µm**:** *p*=0.0015, F=22.08; 20µm: *p*=0.0023, F=19.24; 25µm**:** *p*=0.0021, F=19.84, 30µm**:** *p*=0.0021, F=19.87).

While the results from our pharmacological experiments are consistent with Rac1 as the downstream target of Farp2, EHT inhibits all Rac activity (Onesto et al., 2008; Shutes et al., 2007) activity. Using siRNA specific to Rac1, we found that WT cortical neurons transfected with Rac1 siRNA not only expressed a significantly lower level of Rac1 (**Fig. 9A-B**, Student t-test t=4.245, *p*=0.0132), but were also non-responsive to Sema3A-induced dendrite outgrowth and branching compared to the Sema3A-scramble siRNA (**Fig. 9C-G**; two-way ANOVA **Sholl**: 15µm: *p*=0.0111, F=10.81; 20µm: *p*=0.0032, F=17.16; 25µm: *p*=0.0026, F=18.48; 30µm: *p*=0.0047, F=15.08; 35µm: *p*=0.0055, F=14.14; **Length**: *p*<0.0001, F=112.6; **DCI**: *p*<0.0001, F=70.5; **Dendritic tips**: p=0.0006, F=29.49). Finally, we asked whether Rac1 activity is altered following Sema3A signaling in primary cortical neurons. Using a biochemical assay to pull down the downstream target of Rac1, PAK1, we quantified the level of active Rac1 in its GTP bound state (see details in Materials and Methods). We found that the level of Rac1-GTP increased in WT primary cortical neurons following 30 minutes treatment with alkaline phosphatase (AP) tagged-Sema3A compared to the vehicle control AP treatment (Student's t-test t=3.168, *p*=0.0339). Moreover, we found that Sema3A treatment on *PlxnA4*$^{KRK\text{-}AAA}$ and on *Farp2* KO cortical neurons did not induce any significant increase in Rac1 activity (**Fig. 9H-I**, One way ANOVA p=0.0022; F=20.14). Taken together, our results demonstrate that Sema3A-induced

cortical neuron dendrite elaboration requires the activation of the PlxnA4^{KRK} motif, which signals through Farp2 GEF to activate Rac1.

Discussion

How a finite number of molecular cues can sculpt the precise neuronal connections of complex circuits and induce diverse cellular responses is a fundamental question in neural development. Here, we show that Sema3A signals through the PlxnA4 receptor by selectively engaging the cytoplasmic KRK motif to specifically promote cortical neuron basal dendrite elaboration, but not CNS or PNS axon guidance. Although we cannot completely rule out the involvement of another co-receptor, which interacts with PlxnA4 in a KRK-dependent manner, currently there is no evidence supporting this notion. Our work supports the hypothesis that this KRK sequence is a signaling motif. First, Farp2 interacts with PlxnA4 in a KRK-dependent manner (Mlechkovich et al., 2014). Second, *PlxnA4*$^{KRK\text{-}AAA}$ and *Farp2* interact genetically *in vivo*. Additionally, this PlxnA4-Farp2 pathway requires the downstream target of Farp2, the small GTPase Rac1, to be active in cortical neurons but not in DRG sensory axons. Taken together, our results uncovered, for the first time, the selective Sema3A pathway through the KRK motif of the PlxnA4 receptor that activates Farp2-Rac1 signaling to control dendrite morphogenesis specifically in layer 5 cortical neurons (**Fig. 10**). In agreement with our work, a recent study suggested a functional divergence of the PlexinB motifs in the *Drosophila* olfactory circuit (Guajardo et al., 2019). Unlike our study, the downstream elements to these PlexinB motifs remain elusive.

PlxnA4-Farp2-Rac1 pathway is required for dendrite morphogenesis but not for axon guidance

Our *in vitro* and *in vivo* analyses of the *PlxnA4*$^{KRK\text{-}AAA}$ mouse agree with our previous overexpression studies of PlxnA4 mutants in cultured neurons (Mlechkovich et al., 2014). While our previous study showed that Sema3A-mediated axon growth cone collapse is disrupted by

Farp2 siRNA knockdown in DRG neurons, our current results using the *Farp2* KO mouse contradicts the *in vitro* knockdown findings. The basis for this difference may be due to off-target effects of the siRNA or compensatory mechanisms in the *Farp2* KO DRGs. Another study argued that Sema3A signaling mediates the dissociation of Farp2 from PlexinA1, resulting in the activation of Rac1 by Farp2 in axon repulsion assays of chick DRG neurons (Toyofuku et al., 2005). We have not found any evidence that this pathway is required for DRG axonal repulsion *in vitro* or for any repulsive guidance events of different neuronal types *in vivo*. Although there might be species differences between mice and chicken in Sema3A downstream signaling that may account for these discrepancies. Our data support the model that this pathway is exclusively required for dendrite morphogenesis (**Fig. 10**).

While previous studies showed that Sema3A could increase Rac1 activity, they were mainly performed with either COS7 or HEK 293 cells (Toyofuku et al., 2005; Turner et al., 2004). We showed for the first time that Sema3A signaling in cortical neurons increases Rac1 activity. Another study using Rac1 siRNA in non-stimulated hippocampal neurons showed impairment in dendrite but not axon development (Gualdoni et al., 2007). In contrast, our data suggest that in cortical neurons Rac1 is needed for Sema3A-induced dendritic elaboration but not in the basal state. Furthermore, we corroborated our knockdown findings by inhibiting Rac1 activity with a pan-Rac inhibitor (EHT1864), which only perturbed Sema3A-mediated dendritic elaboration but not axonal growth cone collapse. While our results cannot rule out the contribution of other Rac isoforms (Rac2, Rac3 and RhoG), there are several reasons to support Rac1 as the favorite candidate. First, Rac2 expression has been shown to be restricted to hematopoietic cells (Roberts et al., 1999). Second, it has been proposed that Rac1 and Rac3 have opposing roles. While Rac1 is localized to the plasma membrane and cell protrusions, required for cell differentiation, neurite outgrowth, and involved in dendrites and spines development and maintenance (Gonzalez-Billault et al., 2012; Luo, 2000), Rac3 is localized in the perinuclear region, required for maintaining an undifferentiated state and interferes with

integrin-mediated cell-matrix adhesions (Corbetta et al. 2005; Hajdo-Milasinovic et al., 2007; Hajdo-Milasinovic et al., 2009; Waters et al. 2008). The least studied is RhoG, which is expressed broadly (de Curtis, 2008) and previously shown to reduce dendrite complexity in hippocampal neurons (Franke et al., 2012; Schulz et al., 2016), rather than promoting dendritic arborization like our Rac1 results. Taken together, both *in vitro* and *in vivo* results support PlxnA4^{KRK}-Farp2-Rac1 as the main pathway in Sema3A-mediated signaling in cortical neuron dendrite morphogenesis.

How is the specificity of the PlxnA4-Farp2-Rac1 pathway in cortical neuron dendritic morphogenesis achieved? One simple explanation is differential gene expression. However, all the components of this pathway are expressed both in cortical and DRG neurons during development (Mlechkovich et al., 2014). Another possibility is that the KRK motif is inaccessible to Farp2 in DRG neurons. While beyond the scope of this study, this may be achieved by another FERM domain-containing protein, which is not required for signaling, or by differential lipid composition of the axons and dendrites membranes, as the KRK motif is located adjacent to the transmembrane domain.

Sema3A signaling as a mechanism for promoting dendrite morphogenesis and remodeling in CNS neurons

Previous studies have identified the Src kinases (SFKs) as downstream effectors of Sema3A signaling in cortical basal dendrite elaboration (Morita et al., 2006; Sasaki et al. 2002). Recently, the protein tyrosine phosphatase δ (Ptpδ) was shown to interact with Nrp1 and to regulate the activity of SFKs in cortical neurons (Nakamura et al., 2017). However, these studies also demonstrated that the SFKs and Ptpδ control the growth cone collapse response mediated by Sema3A (Nakamura et al., 2017; Sasaki et al. 2002). Therefore, the SFKs do not confer

functional specificity, but rather they may be considered as non-specific signaling elements that are required for any type of Sema3A function.

While Sema3A can promote dendrite branching in dissociated hippocampal neurons (Fenstermaker et al., 2004), it also regulates the polarization of axon versus dendrite during hippocampal development (Shelly et al., 2011). Exogenous application of Sema3A suppressed undifferentiated neurites from differentiating into axons and promoted dendrite growth by elevating and reducing cGMP and cAMP levels, respectively. The ability of Sema3A to induce dendrite differentiation versus axon formation is recapitulated in *Xenopus* spinal neurons (Nishiyama et al., 2011). While the mechanism is unclear, Sema3A treatment of *Xenopus* spinal interneurons induced dendrite identity specification by simultaneous suppression of axon identity through regulation of cGMP signaling and voltage-sensitive Ca^{2+} channel $Ca_V2.3$ expression. Activity-dependent Sema3A-induced dendrite branching is an interesting notion. Using an overexpression paradigm with tagged Farp1, Nrp1 and PlxnA1, another study showed the other member of the FERM domain containing RhoGEF Farp1 can associate with Nrp1/PlxnA1 complexes in HEK293 cells (Cheadle and Biederer, 2014). While Sema3A treatment of 21 days *in vitro* hippocampal neurons was unable to induce dendrite branching when Farp1 was knocked-down in the presence of TTX, overexpression of PlxnA1 with TTX resulted in increased length of total dendritic branches, suggesting that the semaphorin signaling pathway in hippocampal neurons is different than in cortical neurons, which we show to be Sema3A-Nrp1/PlxnA4-Farp2-Rac1.

Overall, our study uncovers $PlxnA4^{KRK}$/Farp2/Rac1 as a selective signaling pathway towards cortical pyramidal dendritic elaboration. Broadly, our results shed light on a long-standing question regarding the ability of multifunctional receptors to trigger diverse outputs, by demonstrating how distinct morphological changes can be pin pointed to specific receptor signaling motifs and their downstream effectors.

Author Contributions:

A.Y. and T.S.T conceived the study; V.D. and R.G. contributed equally to this study and performed most of the experiments; E.M, I.G. and K.W. assisted with some of the experiments, assisted with the generation of the new mutant mouse lines and animal husbandry work. V.D., R.G., A.Y. and T.S.T. contributed to the experimental design, interpretation of the results, and wrote the manuscript.

References:

Anzo, M., Sekine, S., Makihara, S., Chao, K., Miura, M., and Chihara, T. (2017). Dendritic Eph organizes dendrodendritic segregation in discrete olfactory map formation in Drosophila. Genes & development *31*, 1054-1065.

Barnes, A.P., and Polleux, F. (2009). Establishment of axon-dendrite polarity in developing neurons. Annu Rev Neurosci *32*, 347-381.

Bradford, M.M. (1976). A rapid and sensitive method for the quantitation of microgram quantities of protein utilizing the principle of protein-dye binding. Analytical biochemistry *72*, 248-254.

Castellani, V., Chedotal, A., Schachner, M., Faivre-Sarrailh, C., and Rougon, G. (2000). Analysis of the L1-deficient mouse phenotype reveals cross-talk between Sema3A and L1 signaling pathways in axonal guidance. Neuron *27*, 237-249.

Chari, R., Mali, P., Moosburner, M., and Church, G.M. (2015). Unraveling CRISPR-Cas9 genome engineering parameters via a library-on-library approach. Nat Methods *12*, 823-826.

Chauvet, S., Cohen, S., Yoshida, Y., Fekrane, L., Livet, J., Gayet, O., Segu, L., Buhot, M.C., Jessell, T.M., Henderson, C.E.*, et al.* (2007). Gating of Sema3E/PlexinD1 signaling by neuropilin-1 switches axonal repulsion to attraction during brain development. Neuron *56*, 807-822.

Cheadle, L., and Biederer, T. (2014). Activity-dependent regulation of dendritic complexity by semaphorin 3A through Farp1. J Neurosci *34*, 7999-8009.

Corbetta, S., Gualdoni, S., Albertinazzi, C., Paris, S., Croci, L., Consalez, G.G., and de Curtis, I. (2005). Generation and characterization of Rac3 knockout mice. Mol Cell Biol *25*, 5763-5776.

de Curtis, I. (2008). Functions of Rac GTPases during neuronal development. Dev Neurosci *30*, 47-58.

Doench, J.G., Fusi, N., Sullender, M., Hegde, M., Vaimberg, E.W., Donovan, K.F., Smith, I., Tothova, Z., Wilen, C., Orchard, R.*, et al.* (2016). Optimized sgRNA design to maximize activity and minimize off-target effects of CRISPR-Cas9. Nat Biotechnol *34*, 184-191.

Doench, J.G., Hartenian, E., Graham, D.B., Tothova, Z., Hegde, M., Smith, I., Sullender, M., Ebert, B.L., Xavier, R.J., and Root, D.E. (2014). Rational design of highly active sgRNAs for CRISPR-Cas9-mediated gene inactivation. Nat Biotechnol *32*, 1262-1267.

Fenstermaker, V., Chen, Y., Ghosh, A., and Yuste, R. (2004). Regulation of dendritic length and branching by semaphorin 3A. J Neurobiol *58*, 403-412.

Ferreira, T.A., Blackman, A.V., Oyrer, J., Jayabal, S., Chung, A.J., Watt, A.J., Sjostrom, P.J., and van Meyel, D.J. (2014). Neuronal morphometry directly from bitmap images. Nat Methods *11*, 982-984.

Franke, K., Otto, W., Johannes, S., Baumgart, J., Nitsch, R., and Schumacher, S. (2012). miR-124-regulated RhoG reduces neuronal process complexity via ELMO/Dock180/Rac1 and Cdc42 signalling. EMBO J *31*, 2908-2921.

Gaitanos, T.N., Koerner, J., and Klein, R. (2016). Tiam-Rac signaling mediates trans-endocytosis of ephrin receptor EphB2 and is important for cell repulsion. J Cell Biol *214*, 735-752.

Gonzalez-Billault, C., Munoz-Llancao, P., Henriquez, D.R., Wojnacki, J., Conde, C., and Caceres, A. (2012). The role of small GTPases in neuronal morphogenesis and polarity. Cytoskeleton (Hoboken) *69*, 464-485.

Gu, C., Rodriguez, E.R., Reimert, D.V., Shu, T., Fritzsch, B., Richards, L.J., Kolodkin, A.L., and Ginty, D.D. (2003). Neuropilin-1 conveys semaphorin and VEGF signaling during neural and cardiovascular development. Developmental cell *5*, 45-57.

Guajardo, R., Luginbuhl, D.J., Han, S., Luo, L., and Li, J. (2019). Functional divergence of Plexin B structural motifs in distinct steps of Drosophila olfactory circuit assembly. eLife *8*.

Gualdoni, S., Albertinazzi, C., Corbetta, S., Valtorta, F., and de Curtis, I. (2007). Normal levels of Rac1 are important for dendritic but not axonal development in hippocampal neurons. Biol Cell *99*, 455-464.

Hajdo-Milasinovic, A., Ellenbroek, S.I., van Es, S., van der Vaart, B., and Collard, J.G. (2007). Rac1 and Rac3 have opposing functions in cell adhesion and differentiation of neuronal cells. J Cell Sci *120*, 555-566.

Hajdo-Milasinovic, A., van der Kammen, R.A., Moneva, Z., and Collard, J.G. (2009). Rac3 inhibits adhesion and differentiation of neuronal cells by modifying GIT1 downstream signaling. J Cell Sci *122*, 2127-2136.

He, X., Kuo, Y.C., Rosche, T.J., and Zhang, X. (2013). Structural basis for autoinhibition of the guanine nucleotide exchange factor FARP2. Structure *21*, 355-364.

Hsu, P.D., Scott, D.A., Weinstein, J.A., Ran, F.A., Konermann, S., Agarwala, V., Li, Y., Fine, E.J., Wu, X., Shalem, O.*, et al.* (2013). DNA targeting specificity of RNA-guided Cas9 nucleases. Nat Biotechnol *31*, 827-832.

Huber, A.B., Kania, A., Tran, T.S., Gu, C., De Marco Garcia, N., Lieberam, I., Johnson, D., Jessell, T.M., Ginty, D.D., and Kolodkin, A.L. (2005). Distinct roles for secreted semaphorin signaling in spinal motor axon guidance. Neuron *48*, 949-964.

Huber, A.B., Kolodkin, A.L., Ginty, D.D., and Cloutier, J.F. (2003). Signaling at the growth cone: ligand-receptor complexes and the control of axon growth and guidance. Annu Rev Neurosci *26*, 509-563.

Jan, Y.N., and Jan, L.Y. (2010). Branching out: mechanisms of dendritic arborization. Nat Rev Neurosci *11*, 316-328.

Jin, Z., and Strittmatter, S.M. (1997). Rac1 mediates collapsin-1-induced growth cone collapse. J Neurosci *17*, 6256-6263.

Kantor, D.B., Chivatakarn, O., Peer, K.L., Oster, S.F., Inatani, M., Hansen, M.J., Flanagan, J.G., Yamaguchi, Y., Sretavan, D.W., Giger, R.J.*, et al.* (2004). Semaphorin 5A is a bifunctional axon guidance cue regulated by heparan and chondroitin sulfate proteoglycans. Neuron *44*, 961-975.

Kolodkin, A.L., and Tessier-Lavigne, M. (2011). Mechanisms and molecules of neuronal wiring: a primer. Cold Spring Harb Perspect Biol *3*.

Kubo, T., Yamashita, T., Yamaguchi, A., Sumimoto, H., Hosokawa, K., and Tohyama, M. (2002). A novel FERM domain including guanine nucleotide exchange factor is involved in Rac signaling and regulates neurite remodeling. J Neurosci *22*, 8504-8513.

Lom, B., and Cohen-Cory, S. (1999). Brain-derived neurotrophic factor differentially regulates retinal ganglion cell dendritic and axonal arborization in vivo. J Neurosci *19*, 9928-9938.

Luo, L. (2000). Rho GTPases in neuronal morphogenesis. Nat Rev Neurosci *1*, 173-180.

Mlechkovich, G., Peng, S.S., Shacham, V., Martinez, E., Gokhman, I., Minis, A., Tran, T.S., and Yaron, A. (2014). Distinct cytoplasmic domains in Plexin-A4 mediate diverse responses to semaphorin 3A in developing mammalian neurons. Science signaling *7*, ra24.

Morita, A., Yamashita, N., Sasaki, Y., Uchida, Y., Nakajima, O., Nakamura, F., Yagi, T., Taniguchi, M., Usui, H., Katoh-Semba, R.*, et al.* (2006). Regulation of dendritic branching and spine maturation by semaphorin3A-Fyn signaling. J Neurosci *26*, 2971-2980.

Nagel, A.N., Marshak, S., Manitt, C., Santos, R.A., Piercy, M.A., Mortero, S.D., Shirkey-Son, N.J., and Cohen-Cory, S. (2015). Netrin-1 directs dendritic growth and connectivity of vertebrate central neurons in vivo. Neural development *10*, 14.

Nakamura, F., Okada, T., Shishikura, M., Uetani, N., Taniguchi, M., Yagi, T., Iwakura, Y., Ohshima, T., Goshima, Y., and Strittmatter, S.M. (2017). Protein Tyrosine Phosphatase delta

Mediates the Sema3A-Induced Cortical Basal Dendritic Arborization through the Activation of Fyn Tyrosine Kinase. J Neurosci *37*, 7125-7139.

Nishiyama, M., Togashi, K., von Schimmelmann, M.J., Lim, C.S., Maeda, S., Yamashita, N., Goshima, Y., Ishii, S., and Hong, K. (2011). Semaphorin 3A induces CaV2.3 channel-dependent conversion of axons to dendrites. Nat Cell Biol *13*, 676-685.

Onesto, C., Shutes, A., Picard, V., Schweighoffer, F., and Der, C.J. (2008). Characterization of EHT 1864, a novel small molecule inhibitor of Rac family small GTPases. Methods in enzymology *439*, 111-129.

Peng, S.S., and Tran, T.S. (2017). Regulation of Cortical Dendrite Morphology and Spine Organization by Secreted Semaphorins: A Primary Culture Approach. Methods Mol Biol *1493*, 209-222.

Riccomagno, M.M., Hurtado, A., Wang, H., Macopson, J.G., Griner, E.M., Betz, A., Brose, N., Kazanietz, M.G., and Kolodkin, A.L. (2012). The RacGAP beta2-Chimaerin selectively mediates axonal pruning in the hippocampus. Cell *149*, 1594-1606.

Roberts, A.W., Kim, C., Zhen, L., Lowe, J.B., Kapur, R., Petryniak, B., Spaetti, A., Pollock, J.D., Borneo, J.B., Bradford, G.B.*, et al.* (1999). Deficiency of the hematopoietic cell-specific Rho family GTPase Rac2 is characterized by abnormalities in neutrophil function and host defense. Immunity *10*, 183-196.

Sasaki, Y., Cheng, C., Uchida, Y., Nakajima, O., Ohshima, T., Yagi, T., Taniguchi, M., Nakayama, T., Kishida, R., Kudo, Y.*, et al.* (2002). Fyn and Cdk5 mediate semaphorin-3A signaling, which is involved in regulation of dendrite orientation in cerebral cortex. Neuron *35*, 907-920.

Schulz, J., Franke, K., Frick, M., and Schumacher, S. (2016). Different roles of the small GTPases Rac1, Cdc42, and RhoG in CALEB/NGC-induced dendritic tree complexity. J Neurochem *139*, 26-39.

Shelly, M., Cancedda, L., Lim, B.K., Popescu, A.T., Cheng, P.L., Gao, H., and Poo, M.M. (2011). Semaphorin3A regulates neuronal polarization by suppressing axon formation and promoting dendrite growth. Neuron *71*, 433-446.

Shutes, A., Onesto, C., Picard, V., Leblond, B., Schweighoffer, F., and Der, C.J. (2007). Specificity and mechanism of action of EHT 1864, a novel small molecule inhibitor of Rac family small GTPases. J Biol Chem *282*, 35666-35678.

Smith, C.J., Watson, J.D., VanHoven, M.K., Colon-Ramos, D.A., and Miller, D.M., 3rd (2012). Netrin (UNC-6) mediates dendritic self-avoidance. Nat Neurosci *15*, 731-737.

Stoeckli, E.T. (2018). Understanding axon guidance: are we nearly there yet? Development *145*.

Takegahara, N., Kang, S., Nojima, S., Takamatsu, H., Okuno, T., Kikutani, H., Toyofuku, T., and Kumanogoh, A. (2010). Integral roles of a guanine nucleotide exchange factor, FARP2, in osteoclast podosome rearrangements. FASEB J *24*, 4782-4792.

Tong, Y., Chugha, P., Hota, P.K., Alviani, R.S., Li, M., Tempel, W., Shen, L., Park, H.W., and Buck, M. (2007). Binding of Rac1, Rnd1, and RhoD to a novel Rho GTPase interaction motif destabilizes dimerization of the plexin-B1 effector domain. J Biol Chem *282*, 37215-37224.

Toyofuku, T., Yoshida, J., Sugimoto, T., Zhang, H., Kumanogoh, A., Hori, M., and Kikutani, H. (2005). FARP2 triggers signals for Sema3A-mediated axonal repulsion. Nat Neurosci *8*, 1712-1719.

Tran, T.S., Kolodkin, A.L., and Bharadwaj, R. (2007). Semaphorin regulation of cellular morphology. Annu Rev Cell Dev Biol *23*, 263-292.

Tran, T.S., Rubio, M.E., Clem, R.L., Johnson, D., Case, L., Tessier-Lavigne, M., Huganir, R.L., Ginty, D.D., and Kolodkin, A.L. (2009). Secreted semaphorins control spine distribution and morphogenesis in the postnatal CNS. Nature *462*, 1065-1069.

Turner, L.J., Nicholls, S., and Hall, A. (2004). The activity of the plexin-A1 receptor is regulated by Rac. J Biol Chem *279*, 33199-33205.

Waimey, K.E., Huang, P.H., Chen, M., and Cheng, H.J. (2008). Plexin-A3 and plexin-A4 restrict the migration of sympathetic neurons but not their neural crest precursors. Dev Biol *315*, 448-458.

Waters, J.E., Astle, M.V., Ooms, L.M., Balamatsias, D., Gurung, R., and Mitchell, C.A. (2008). P-Rex1 - a multidomain protein that regulates neurite differentiation. J Cell Sci *121*, 2892-2903.

Whitford, K.L., Dijkhuizen, P., Polleux, F., and Ghosh, A. (2002). Molecular control of cortical dendrite development. Annu Rev Neurosci *25*, 127-149.

Xu, H., Xiao, T., Chen, C.H., Li, W., Meyer, C.A., Wu, Q., Wu, D., Cong, L., Zhang, F., Liu, J.S.*, et al.* (2015). Sequence determinants of improved CRISPR sgRNA design. Genome Res *25*, 1147-1157.

Yaron, A., Huang, P.H., Cheng, H.J., and Tessier-Lavigne, M. (2005). Differential requirement for Plexin-A3 and -A4 in mediating responses of sensory and sympathetic neurons to distinct class 3 Semaphorins. Neuron *45*, 513-523.

Zanata, S.M., Hovatta, I., Rohm, B., and Puschel, A.W. (2002). Antagonistic effects of Rnd1 and RhoD GTPases regulate receptor activity in Semaphorin 3A-induced cytoskeletal collapse. J Neurosci *22*, 471-477.

Zhao, X.F., Kohen, R., Parent, R., Duan, Y., Fisher, G.L., Korn, M.J., Ji, L., Wan, G., Jin, J., Puschel, A.W.*, et al.* (2018). PlexinA2 Forward Signaling through Rap1 GTPases Regulates Dentate Gyrus Development and Schizophrenia-like Behaviors. Cell Rep *22*, 456-470.

Figure 1. Generation of the *PlxnA4*$^{KRK\text{-}AAA}$ mutant mouse line and the *Farp2* KO mouse line.

A, RT-qPCR analysis revealed unchanged *PlxnA4* mRNA transcript levels in E13.5 *PlxnA4*$^{KRK\text{-}AAA}$ heads compared to WT littermate controls. *PlxnA4* KO heads were

processed as well as a negative control. Quantification was performed using a relative quantification analysis (ΔΔCt) and presented as means ± SEM, Student's t-test. *** p<0.001. **B-C**, Western blot analysis of E13.5 DRGs and cortices extracted from *PlxnA4*$^{KRK\text{-}AAA}$ and WT littermate controls revealed similar Plexin-A4 and Nrp1 protein levels in both genotypes. Heads of E13.5 *PlxnA4* KO were used as a negative control. Data are means ± SEM, Student's t-test. **D**, *PlxnA4*$^{KRK\text{-}AAA}$, WT littermates, and *PlxnA4* KO cortices were subjected to anti-Nrp1 immuno-precipitation and probed using a Plexin-A4 antibody. No change in Nrp1-Plexin-A4 association was detected in the *PlxnA4*$^{KRK\text{-}AAA}$ mutant compared to WT. **E-F**, 7DIV cortical neurons from E13.5 *PlxnA4*$^{KRK\text{-}AAA}$ and WT littermate embryos were subjected to a cell-surface biotinylation assay, followed by western blot probing for Plexin-A4. The total mass of biotinylated proteins in the range of ~120-260kDa, detected and quantified using Streptavidin-HRP, was used as loading control. Data are means ± SEM, Student's t-test. **G**, Primary cortical neurons of *PlxnA4*$^{KRK\text{-}AAA}$, WT littermates, and *PlxnA4* KO embryos were immuno-stained in culture using a Plexin-A4 antibody. Plexin-A4 protein levels and its spatial pattern in the *PlxnA4*$^{KRK\text{-}AAA}$ mutant was comparable to the WT, while virtually no Plexin-A4 was detected in the negative control KO. Scale bar is 25 µm. **H**, Schematic representation of the *Farp2* locus on chromosome 1 (GRCm38-mm10) and the CRISPR-Cas9 knockout design. Two sgRNAs flanking an 18,167bp sequence were used: sgRNA 1 targeted a region upstream of the *Farp2* gene promoter, and sgRNA 2 targeted a sequence in intron 2. P1 and P2 (black triangles) represent primers used for detection of the KO allele in a PCR analysis of genomic DNA, targeting sequences outside of the deletion area (upstream of sgRNA1 and downstream of sgRNA2,

respectively). Similarly, P3 and P4 (gray triangles) represent primers used for detection of the WT allele and were targeted at intron 1. RT 1 and 2 (blue triangles) represent primers used for reverse transcription analysis of *Farp2* gene expression levels; RT 1 targeted a sequence comprised of the 3' of exon 4 and 5' of exon 5, and RT 2 targeted exon 6. **I**, PCR analysis of tail genomic DNA obtained from three E13.5 embryos of a *Farp2* Het x Het cross, using primers 1-4 (P1-4). Lengths of the WT and KO alleles are 551 and 271bp, respectively. +/+, WT; +/-, *Farp2* heterozygous; -/-, *Farp2* knockout. **J**, Reverse transcription analysis of WT (+/+) and KO (-/-) cDNA using either *Farp2* primers RT 1-2, (upper panel), or Actin beta (Actb) primers as internal control (lower panel). Both (**G**) and (**H**) demonstrate a successful knockout of the *Farp2* gene and its transcripts.

Figure 2. *PlxnA4*$^{KRK\text{-}AAA}$ and *Farp2* KO DRG axons show intact Sema3A-dependent responses *in vitro*. **A-H**, DRG explants from WT (**A-B**), *PlxnA4*$^{KRK\text{-}AAA}$ (**C-D**) and *Farp2* KO (**F-G**) E13.5 embryos were grown for 48hr, treated with 0.1, 0.5 or 1nM AP-Sema3A (only 1nM is shown) or control conditioned media and stained using Phalloidin-Rhodamine to visualize growth cone collapse. Arrows indicate intact growth cones and arrowheads indicate collapsed growth cones. Quantification of collapse response (**E** and **H**) as a mean percentage of collapsed growth cones out of the total ± SEM; N.S., non-significant; two-way ANOVA with *post hoc* Tukey test. Scale bar, 50µm. **I-M**, Schematic representation of the collagen axonal repulsion assay (**I**), where E13.5 DRG explants from *PlxnA4*$^{KRK\text{-}AAA}$ and WT littermates (**J-K**) or *Farp2* KO and WT littermates (**L-M**) were co-cultured for 48hrs with a COS1 aggregate either secreting myc-Sema3A

(dashed circle) or expressing control PAY1-GFP (green). Cultures were visualized using anti-Tubulin class III immuno-staining. **N**, Quantification of axonal repulsion using the proximal/distal (P/D) ratio, as indicated in (**I**). Data are means ± SEM; N.S., non-significant, Student's t-test. Scale bar, 500µm.

Figure 3. Both *PlxnA4*$^{KRK-AAA}$ and *Farp2* KO neurons are non-responsive to Sema3A-induced cortical neuron dendrite outgrowth *in vitro*. **A**, Representative confocal micrographs of dissociated primary cortical neurons obtained from Wild-Type (WT), *PlxnA4* KO, *PlxnA4*$^{KRK-AAA}$ and *Farp2* KO E13.5 embryos. The neurons were treated with AP or Sema3A 5nM for 24h. **B-E**, Sholl analysis quantified dendritic growth and branching in WT, *PlxnA4* KO, *PlxnA4*$^{KRK-AAA}$ and *Farp2* KO cortical neurons (**B**), measuring the number of dendritic intersections, the total dendritic length (**C**), the DCI (**D**) and the number of dendritic tips (**E**). Data are means, ±SEM from 3 independent cultures of each genotype, two-way ANOVA with post doc Tukey test, $p<0.001$, (*) shows statistic differences. Scale bar, 25µm.

Figure 4. Both *PlxnA4*$^{KRK-AAA}$ and *Farp2* KO cortical neurons are non-responsive even to higher concentrations of Sema3A. A, Representative confocal micrographs of dissociated primary cortical neurons obtained from WT, *PlxnA4*$^{KRK-AAA}$ and *Farp2* KO E13.5 embryos. The WT neurons were treated with AP or Sema3A 5nM and the *PlxnA4*$^{KRK-AAA}$ and *Farp2* KO neurons were treated with AP or Sema3A 10nM for 24h. **B-E**, Sholl analysis quantified dendritic growth and branching in WT, *PlxnA4*$^{KRK-AAA}$ and *Farp2* KO cortical neurons (**B**), measuring the number of dendritic intersections, the

total dendritic length (**C**), the DCI (**D**) and the number of dendritic tips (**E**). Data are means, ±SEM from 3 independent cultures of each genotype, two-way ANOVA with post doc Tukey test, $p<0.001$, (*) shows statistic differences. Scale bar, 25µm.

Figure 5. Reduced basal dendritic arborization in layer 5 cortical neurons from *PlxnA4*$^{KRK\text{-}AAA}$ *and Farp2* KO adult animals. **A**, Golgi stained images of brain (2 to 3 months old) sections of Wild-Type, *PlxnA4* KO, *PlxnA4*$^{KRK\text{-}AAA}$, *Farp2* KO and in *PlxnA4*$^{+/KRK\text{-}AAA}$/*Farp2*$^{+/-}$. **B**, Sholl analysis quantification revealed reduced and altered branching patterns of basal dendrites from layer V cortical neurons in *PlxnA4* KO, *PlxnA4*$^{KRK\text{-}AAA}$, *Farp2* KO and *PlxnA4*$^{+/KRK\text{-}AAA}$/*Farp2*$^{+/-}$ compared to WT and to *PlxnA4*$^{+/KRK\text{-}AAA}$ or *Farp2*$^{+/-}$ littermates. **C-E**, Quantifications of total dendritic length (**C**), DCI (**D**), and dendritic tips (**E**) in all genotype analyzed. Data are means, ±SEM. One-way ANOVA followed by *post hoc* Tukey test. $p < 0.05$. **F-G**, Representative images of the layer 5 cortical neurons and Sholl analysis obtained from a WT, *PlxnA4*$^{KRK\text{-}AAA}$ and *PlxnA4*$^{+/KRK\text{-}AAA}$/*Farp2*$^{+/-}$ Thy1-GFP mice. One-way ANOVA followed by *post hoc* Tukey test. Data are means, ±SEM. n=3 brains/genotype. $p<0.05$, (*) shows statistic difference between WT and *PlxnA4*$^{KRK\text{-}AAA}$ mutant or *PlxnA4* KO or *Farp2* KO; (#) shows statistic difference between WT and *PlxnA4*$^{KRK\text{-}AAA/+}$*Farp2*$^{+/-}$ or *PlxnA4* KO. Scale bar, 25µm for all panels in **A** and **F**.

Figure 6. *PlxnA4*$^{KRK\text{-}AAA}$ and *Farp2* KO animals show normal axonal projections in the PNS and CNS *in vivo*. **A-D**, WT, *PlxnA4*$^{KRK\text{-}AAA}$, *Farp2* KO or *PlxnA4* KO E12.5 embryos were immuno-stained using a Neurofilament antibody to visualize cutaneous

sensory axons pattern. *PlxnA4*$^{KRK\text{-}AAA}$ and *Farp2* KO embryos (**B** and **C**, respectively) were comparable to the WT (**A**), while the *PlxnA4* KO (**D**) exhibited an expected hyperinnervation, including a previously described discrete phenotype (white arrows). Scale bar is 500µm. **E-H** WT, *PlxnA4*$^{KRK\text{-}AAA}$, *Farp2* KO or *PlxnA4* KO E13.5 embryos were immuno-stained using a Tyrosine-hydroxylase antibody to visualize sympathetic axons. *PlxnA4*$^{KRK\text{-}AAA}$ and *Farp2* KO embryos (**F** and **G**, respectively) were comparable to the WT (**E**), while the *PlxnA4* KO (**H**) exhibited an expected medial protrusion of sympathetic axons (black arrows). Scale bar is 250µm. **I-L** WT, *PlxnA4*$^{KRK\text{-}AAA}$, *Farp2* KO or *PlxnA4* KO P30 brains were stained using hematoxylin. *PlxnA4*$^{KRK\text{-}AAA}$ and *Farp2* KO embryos (**J** and **K**, respectively) were comparable to the WT (**I**), while the *PlxnA4* KO (**L**) exhibited an expected disrupted formation of the anterior commissure (white arrows). Scale bar, 500µm.

Figure 7. Inhibition of Rac signaling abolishes Sema3A-mediated cortical neuron dendrite elaboration but does not hinder Sema3A-dependent growth cone collapse of WT or *PlxnA4*$^{KRK\text{-}AAA}$ DRG axons *in vitro*. **A-L**, DRG explants from WT (**A-F**) and *PlxnA4*$^{KRK\text{-}AAA}$ littermates (**G-L**) E13.5 embryos were grown for 48hr, treated for 30min with the pan-Rac inhibitor EHT 1864 at a concentration of 5µM (**B, D, H, J**), 10µM (**C, E, I, K**) or nothing as control (**A, G, F, L**). Then, 1nM Sema3A or control conditioned media was added for 30min (**D-F**, **J-L** and **A-C**, **G-I**, respectively), followed by fixation and Phalloidin-Rhodamine staining for assessment of growth cone collapse. Black arrows indicate intact growth cones and arrowheads indicate collapsed growth cones. **M-N**, Quantification of collapse response as a mean percentage of collapsed

growth cones out of the total ± SEM in WT and *PlxnA4*$^{KRK\text{-}AAA}$ axons, respectively. N.S. – non-significant. Scale bar, 50µm. **O**, Representative confocal micrographs of dissociated primary cortical neurons obtained from WT E13.5 embryos. The neurons were treated with 5nM AP, treated with 5nM Sema3A, 5nM Sema3A+2.5uM EHT, 5nM Sema3A+5uM EHT, and 5nM Sema3A+10uM EHT. **P-S**, Sholl analysis of dendritic intersections (**P**) total dendritic length (**Q**) the DCI (**R**) and number of dendritic tips (**S**), for all treatment conditions described above. Data are means, ±SEM from n=3 independent cultures, two-way ANOVA with post doc Tukey test, $p<0.001$. Scale bar, 25µm for all panels in **A-L** and in all panels in **O**.

Figure 8. Sema3A-dependent dendritic arborization relies on the Farp2 GEF and downstream Rac1 GTPase activation. A, Representative confocal micrographs of dissociated primary neurons obtained from *Farp2* KO animals. The neurons were treated with 5nM AP, treated with 5nM Sema3A, transfected with Farp2-HA cDNA and treated with 5nM AP, transfected with Farp2-HA cDNA and treated with 5nM Sema3A and transfected with Farp2-HA cDNA, treated with 5nM Sema3A+2.5 uM EHT for 24h. **B**, Sholl analysis of dendritic intersections in the 5 different groups. Data are means, ±SEM from n=3 independent cultures, two-way ANOVA with post doc Tukey test, $p<0.01$. (*) shows statistic difference between *Farp2* KO+Farp2-HA and *Farp2* KO+Farp2- HA+Sema3A; (#) shows statistic difference between *Farp2* KO+Farp2-HA+Sema3A and *Farp2* KO+Farp2-HA+Sema3A+EHT. Scale bar, 25µm for all panels in **A**.

Figure 9. Sema3A increases Rac activation in cortical neurons and requires the presence of Rac1 for dendrite elaboration. A, Rac1 specific siRNA decrease Rac1 total protein levels. **B**, Quantification of Rac1 levels, from n=3 independent experiments, Student's t-test, $p<0.05$ (*) shows statistic difference. **C**, Representative confocal micrographs of dissociated primary cortical neurons obtained from WT E13.5 embryos transfected either with scramble siRNA or Rac1 specific siRNA. **D**, Sholl analysis of dendritic intersections; **E**, total dendritic length; **F**, DCI; **G**, number of dendritic tips, for all treatment conditions described above. Data are means, ±SEM from n=3 independent cultures, two-way ANOVA with post doc Tukey test, $p<0.01$, (*) shows statistic difference. Scale bar, 25µm for all panels in **C**. **H**, Pull-down assay showing the effect of 30 min stimulation of Sema3A on Rac1 activation in WT neurons, in *PlxnA4*$^{KRK\text{-}AAA}$ and in *Farp2* KO neurons. **I**, Quantification of Rac1-GTP fold change, from n=3 independent experiments, one Way ANOVA, $p<0.05$ (*) shows statistic difference.

Figure 10. Differential requirement for the KRK motif and its downstream signaling effector Farp2 in Plexin-A4-mediated cellular responses. A, Sema3A-Neuropilin1/PlexinA4 signaling promotes basal dendrite elaboration in deep-layer pyramidal cortical neurons on one hand and growth cone collapse and axonal repulsion on the other. **B**, Substitution of the KRK motif of Plexin-A4 to AAA, ablation of the Plexin-A4-binding effector, the Rac1 GEF Farp2, or inhibition of Rac1 specifically abrogate dendrite elaboration but not growth cone collapse and axonal repulsion.

Figure 1

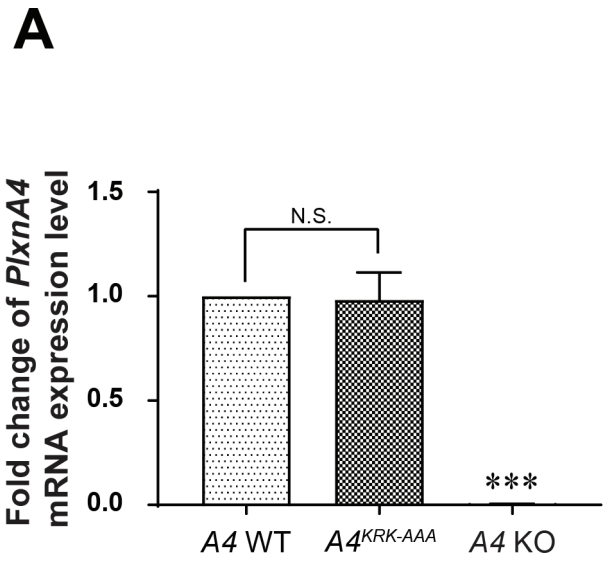

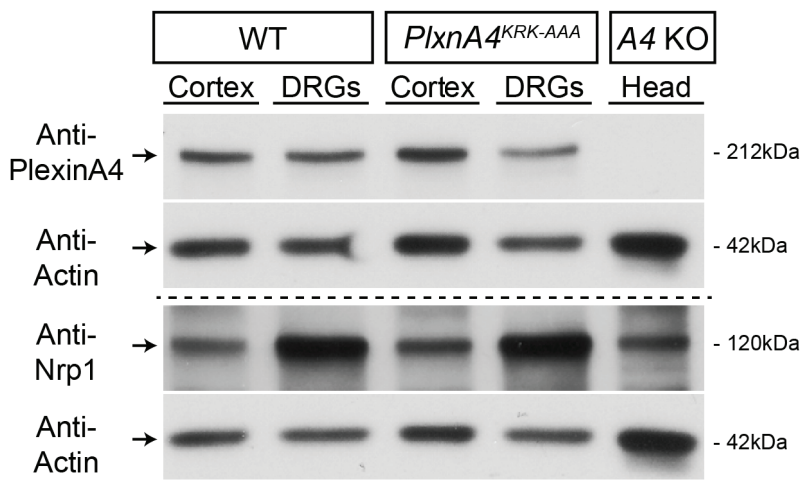

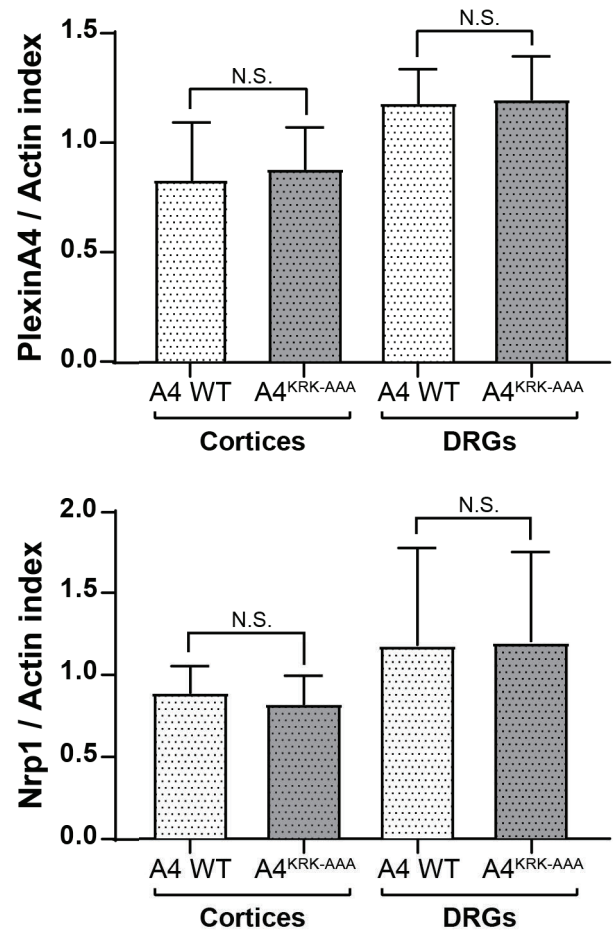

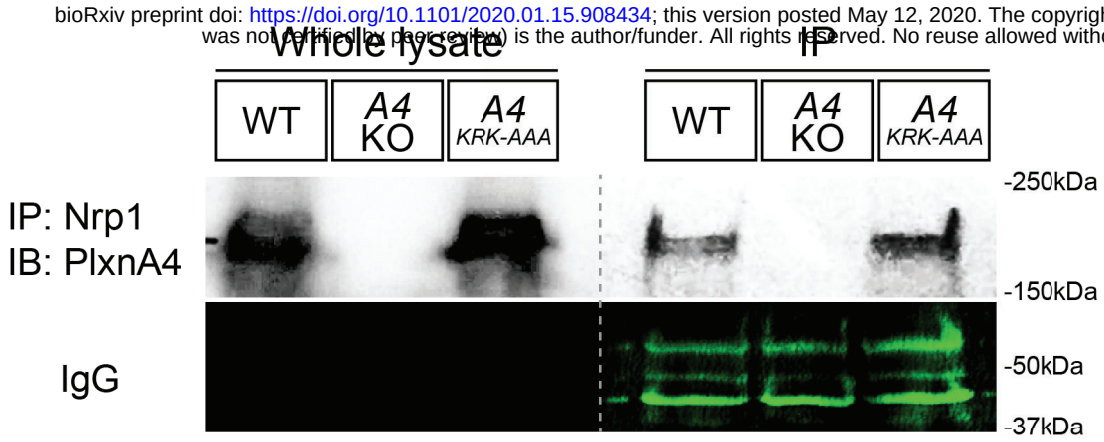

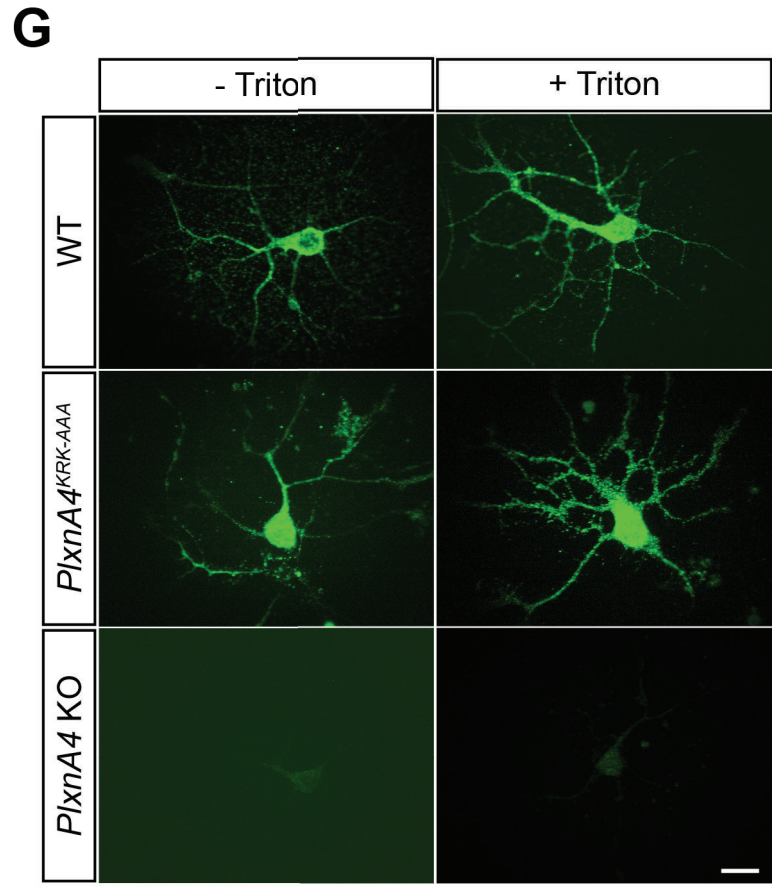

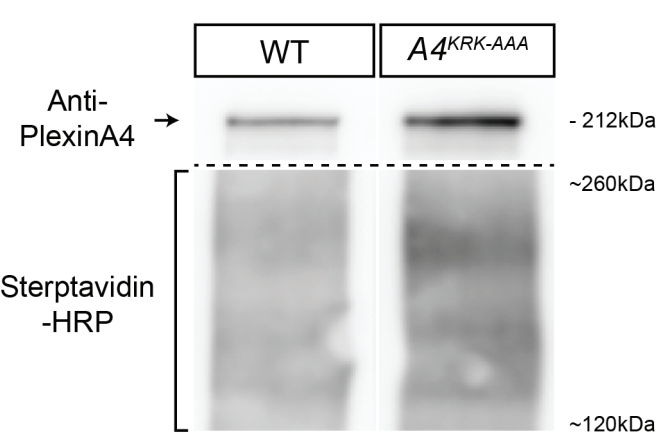

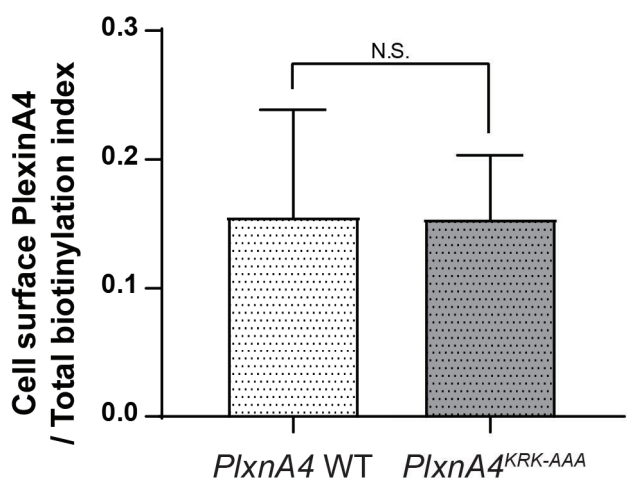

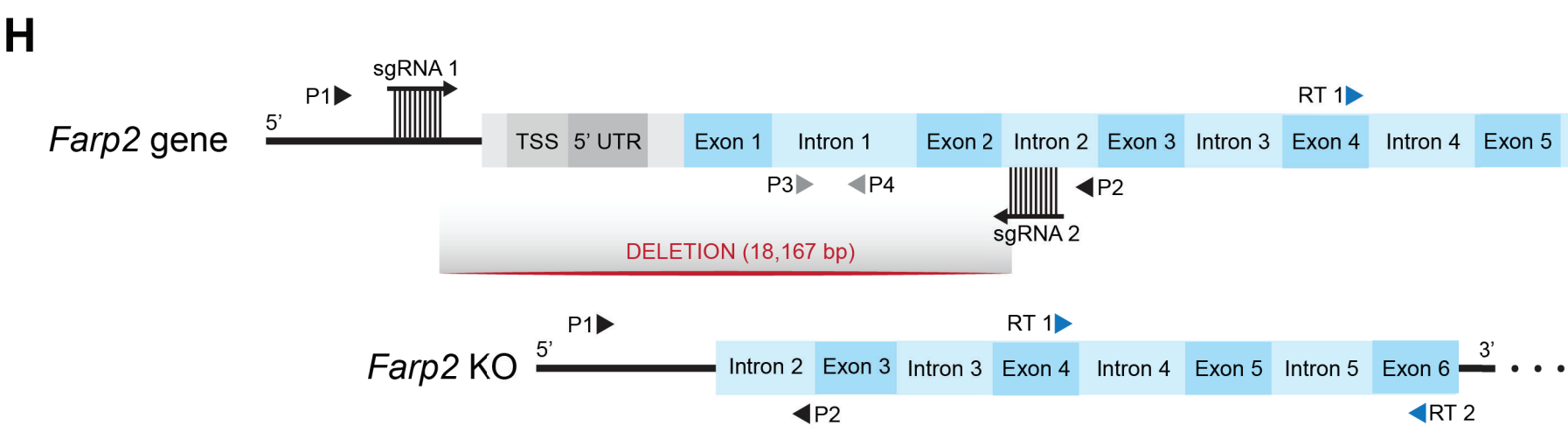

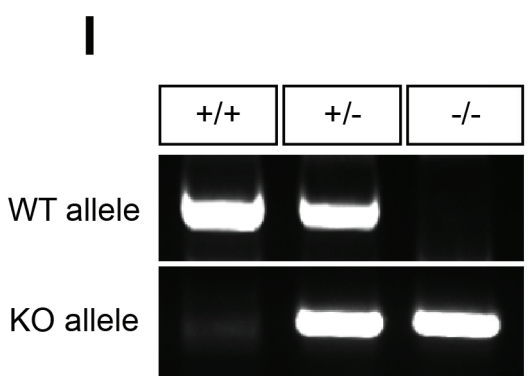

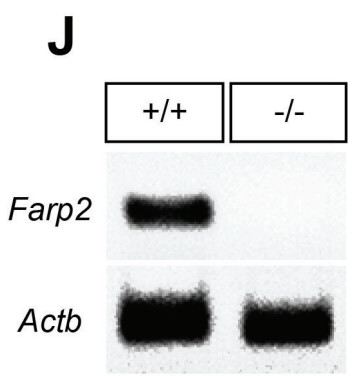

Figure 2

Control | Sema3A 1nM

WT

A B

PlxnA4$^{KRK-AAA}$

C D

Farp2 KO

F G

E

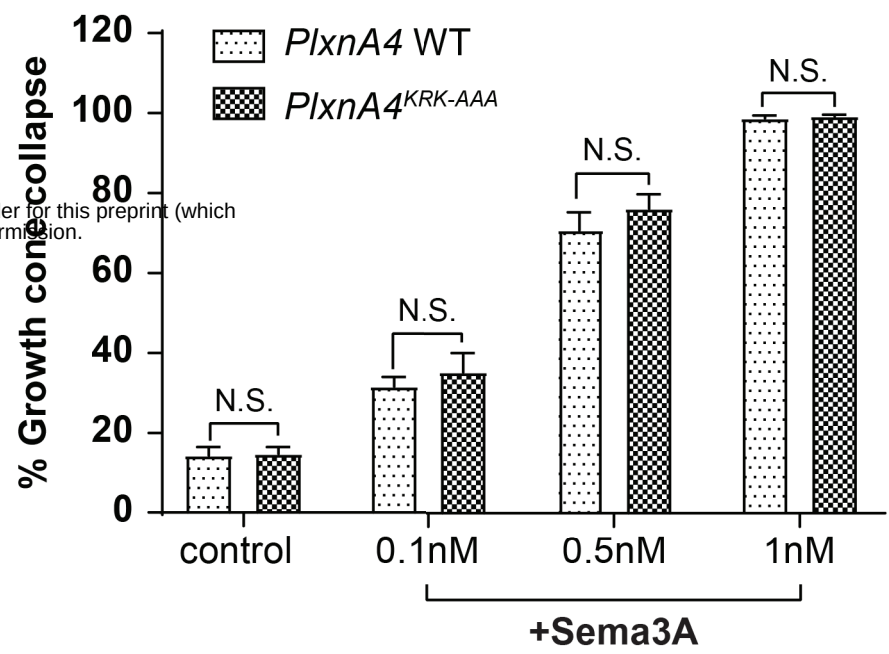

H

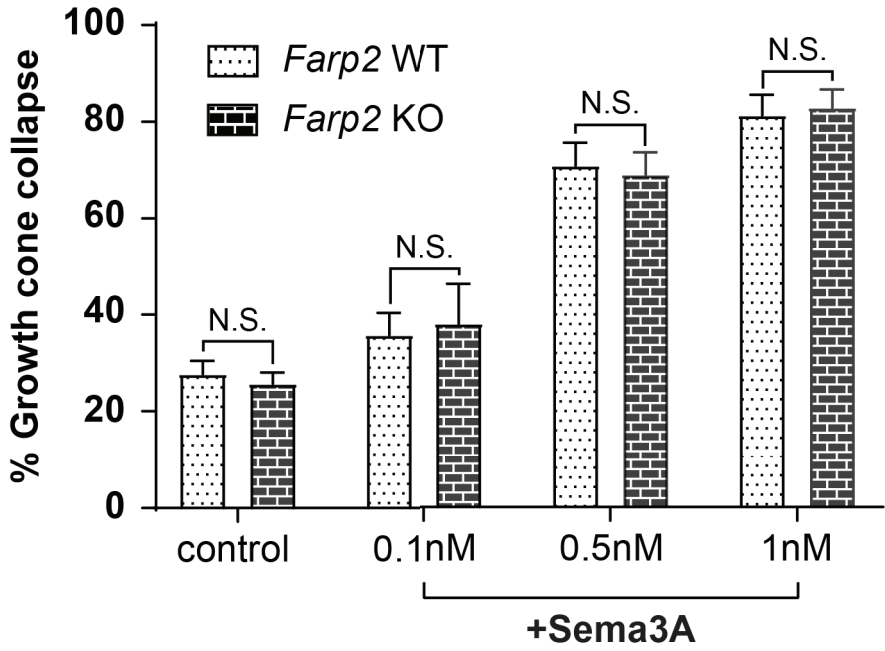

I

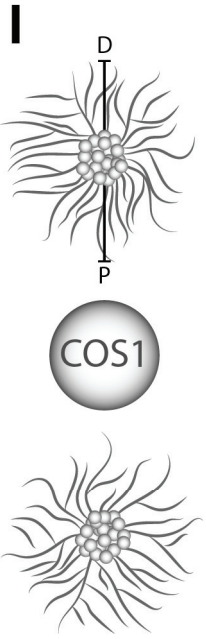

WT | WT

J K L M

Control S3A Control S3A

PlxnA4$^{KRK-AAA}$ | *Farp2* KO

N

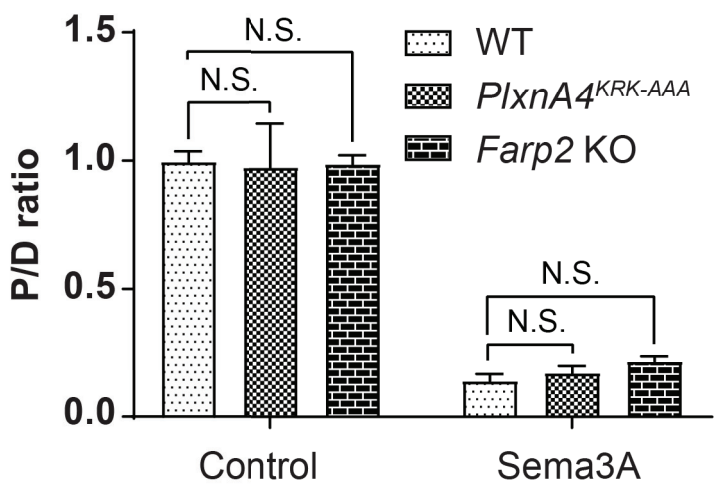

Figure 3

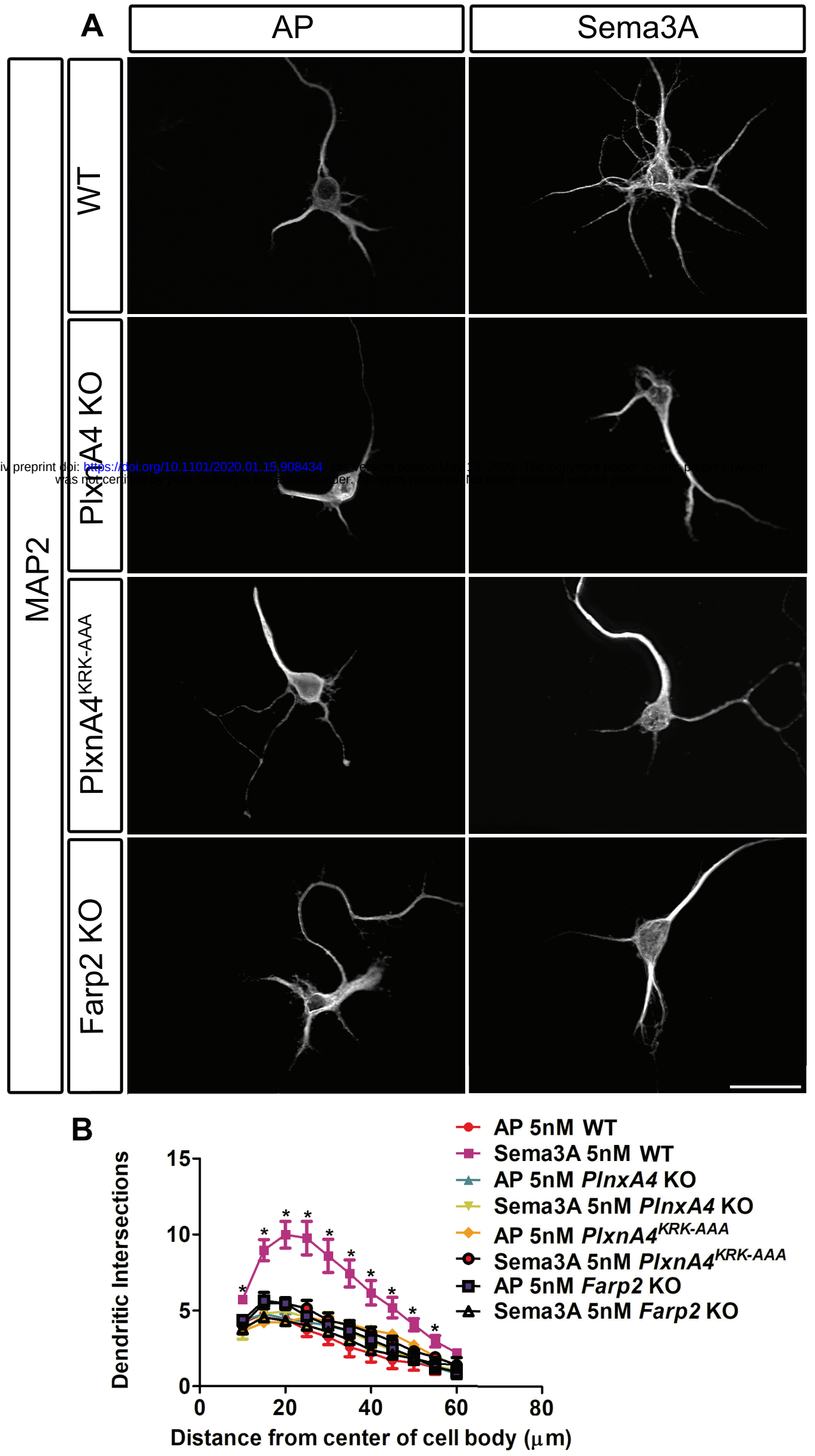

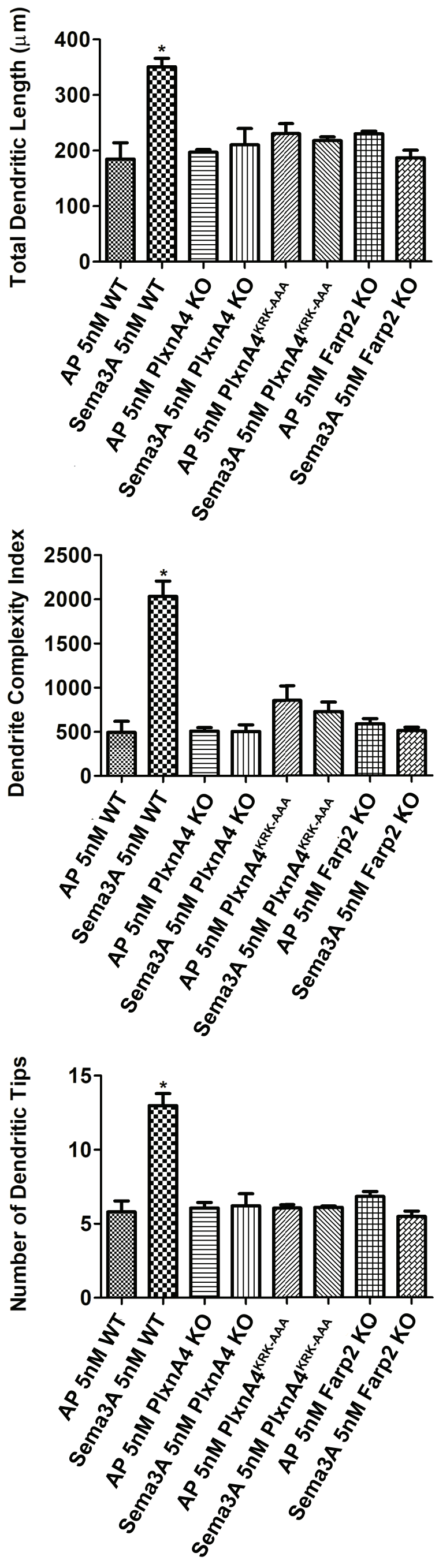

Figure 4

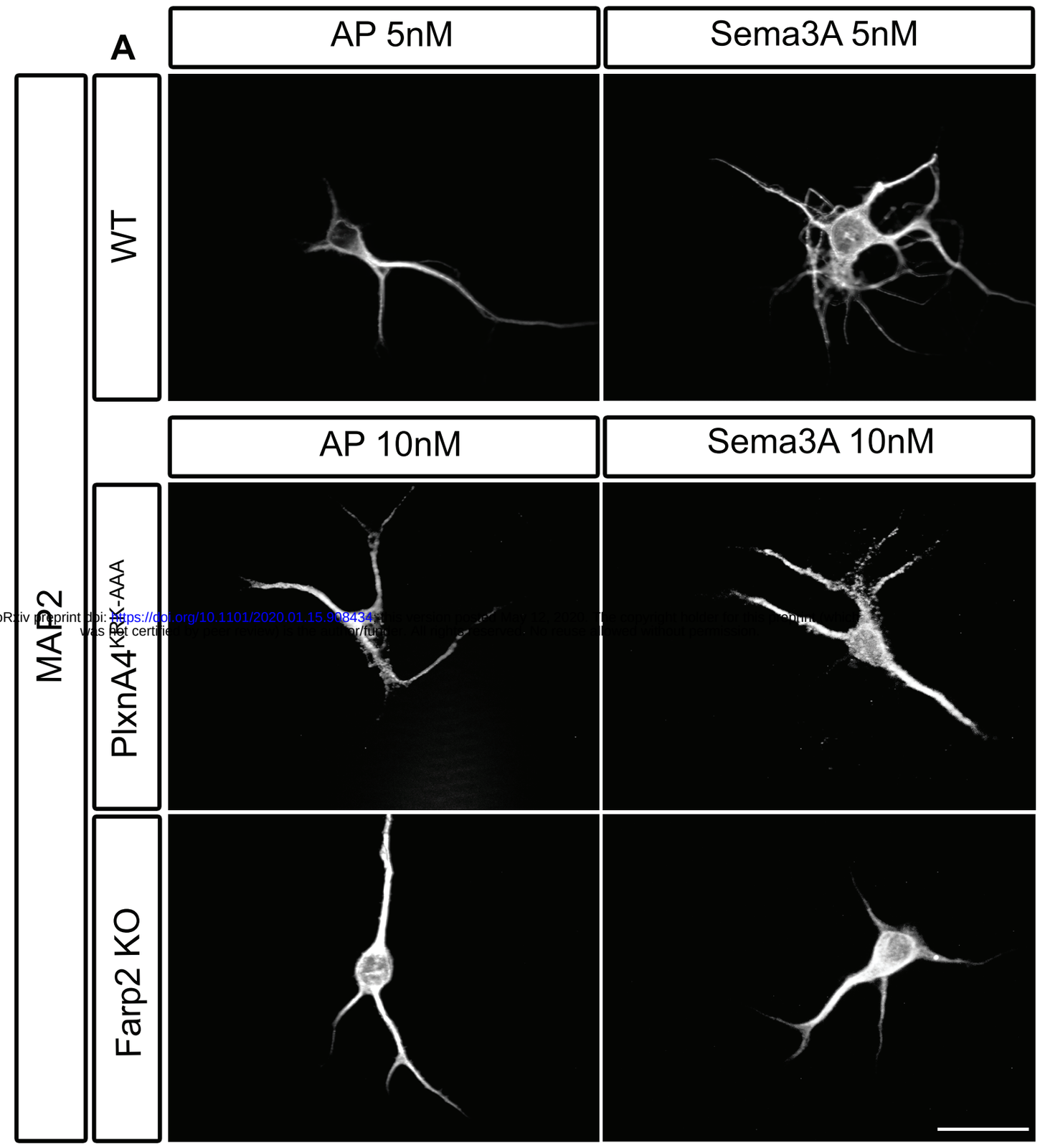

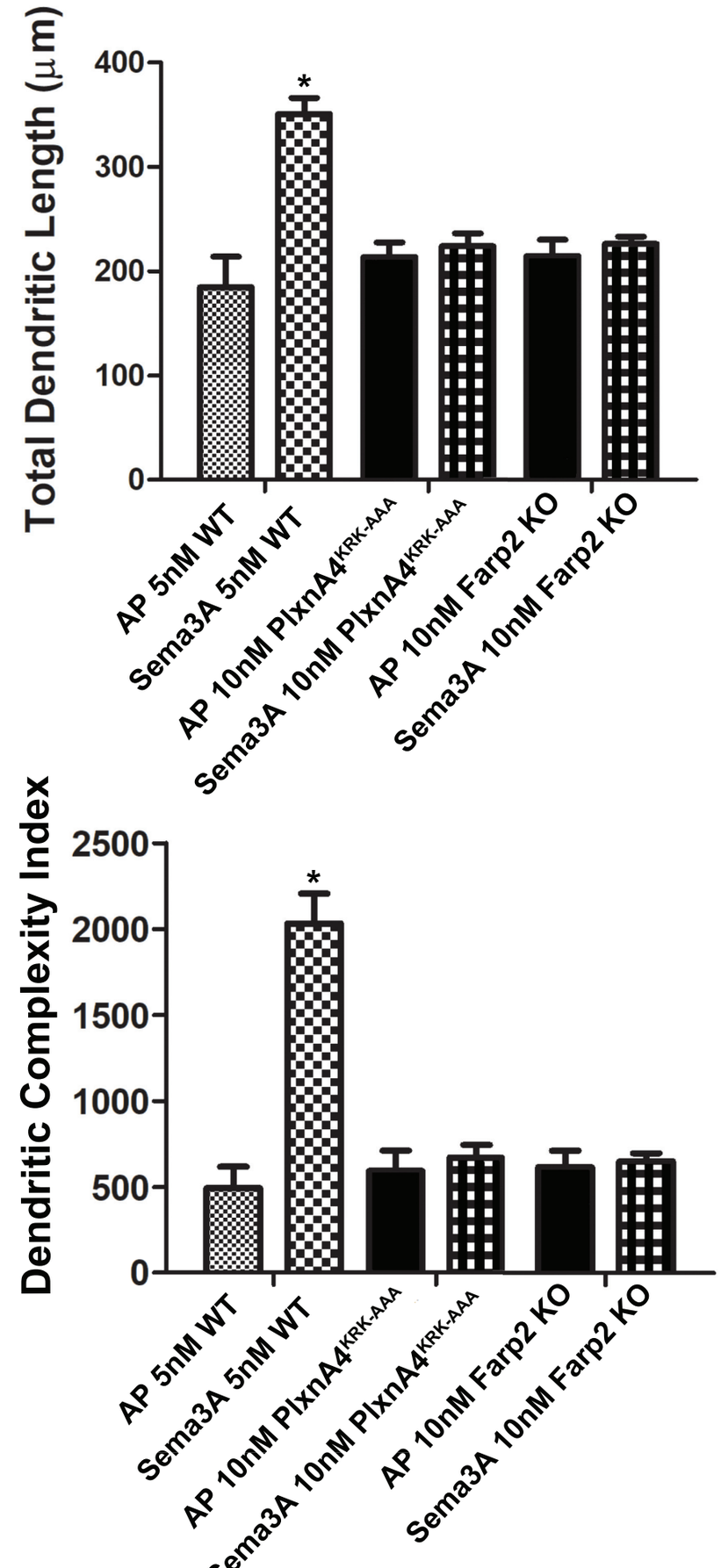

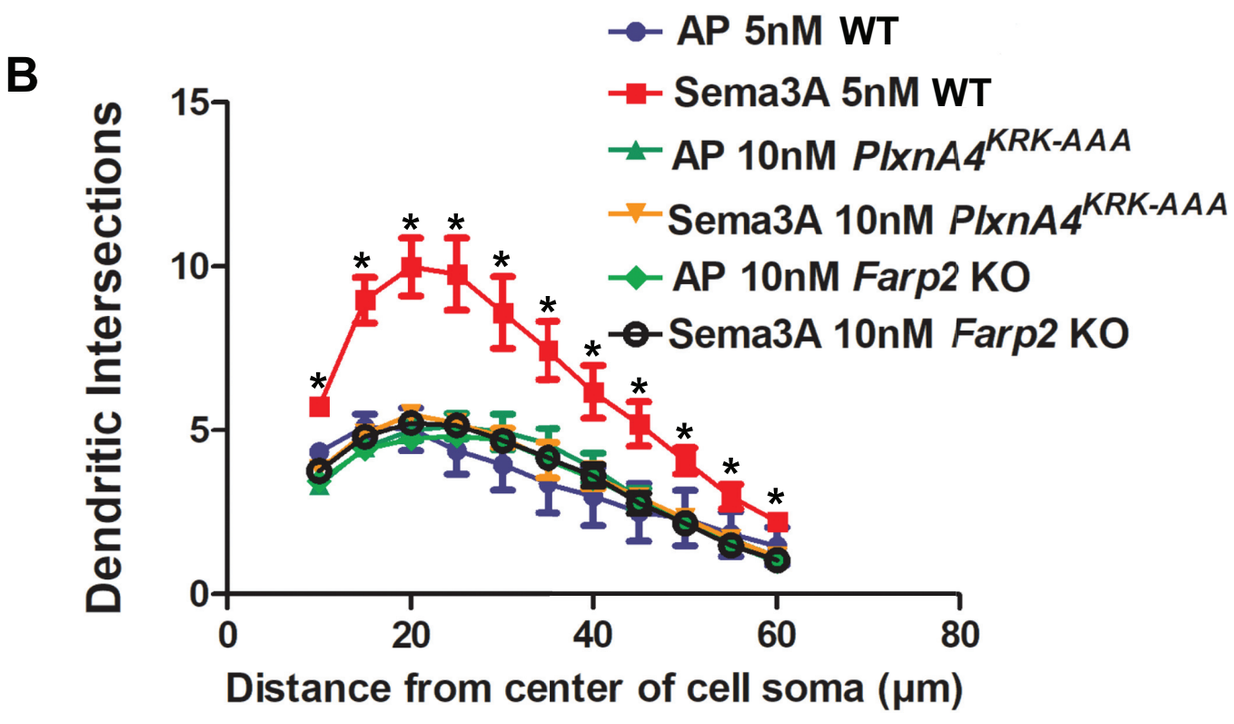

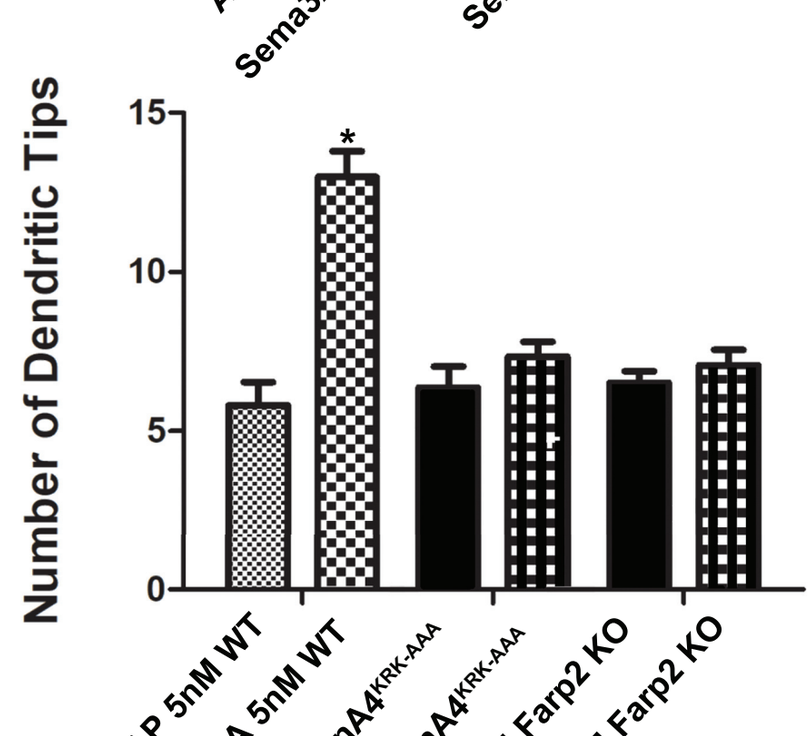

Figure 5

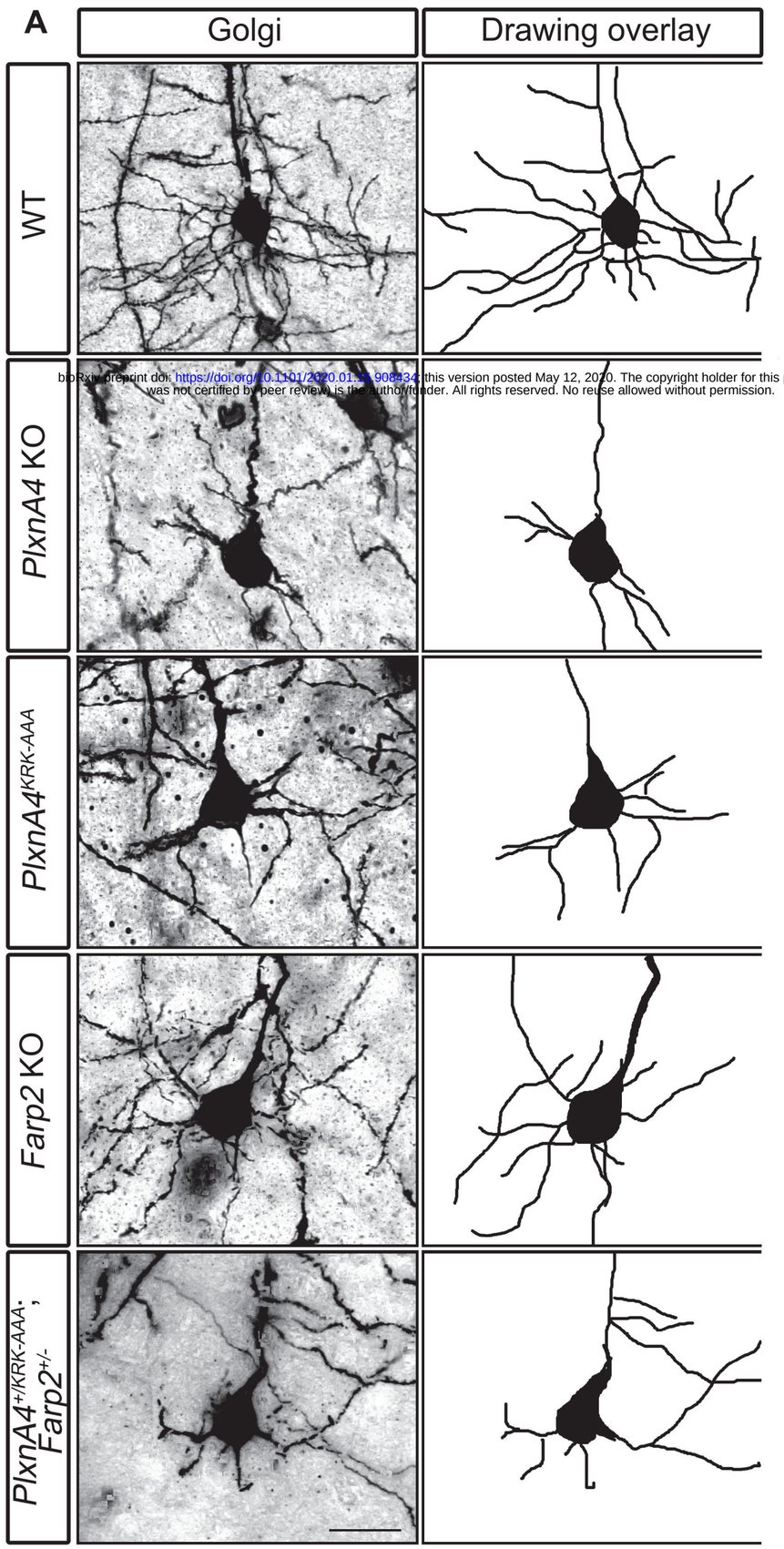

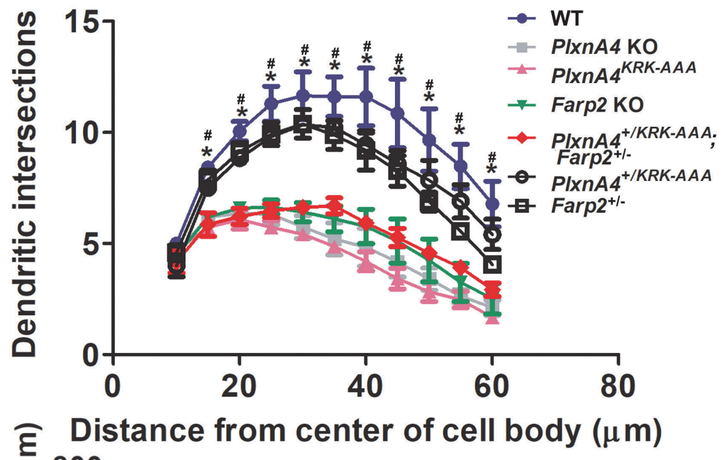

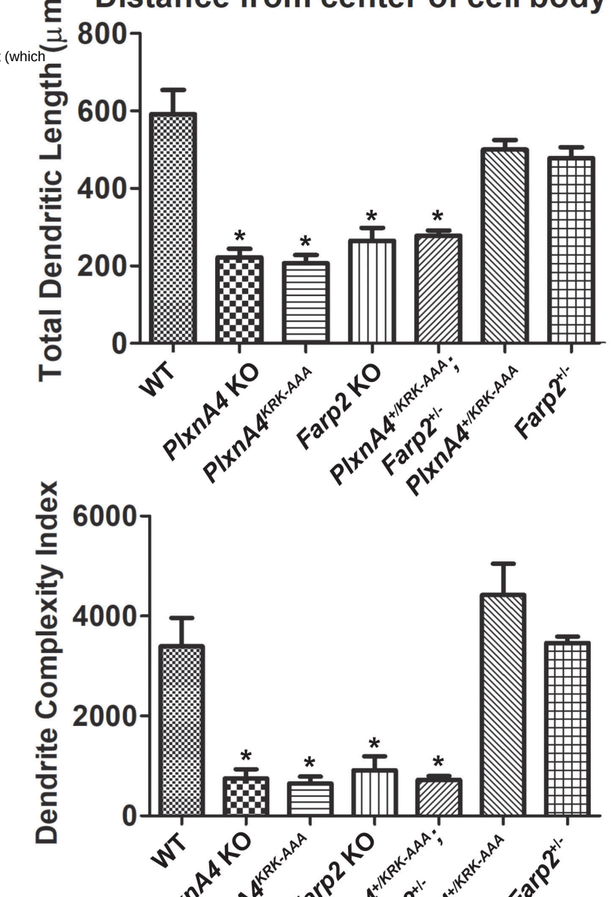

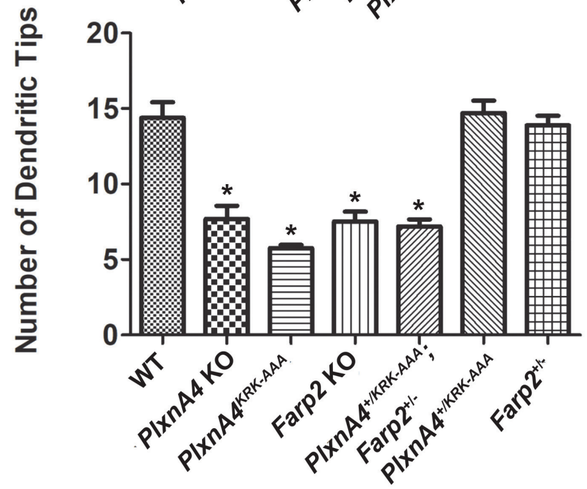

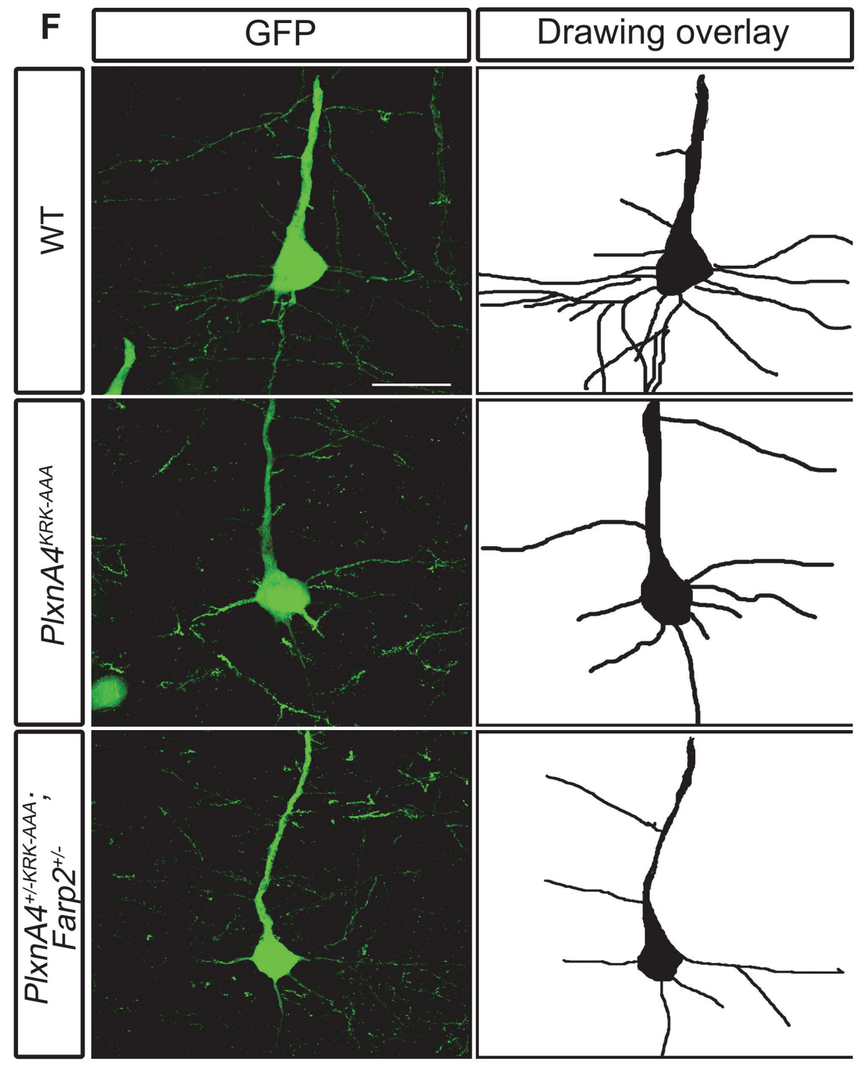

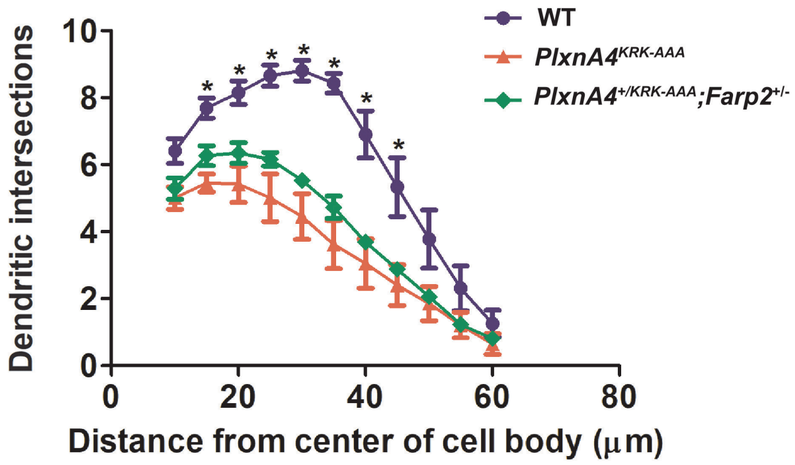

Figure 6

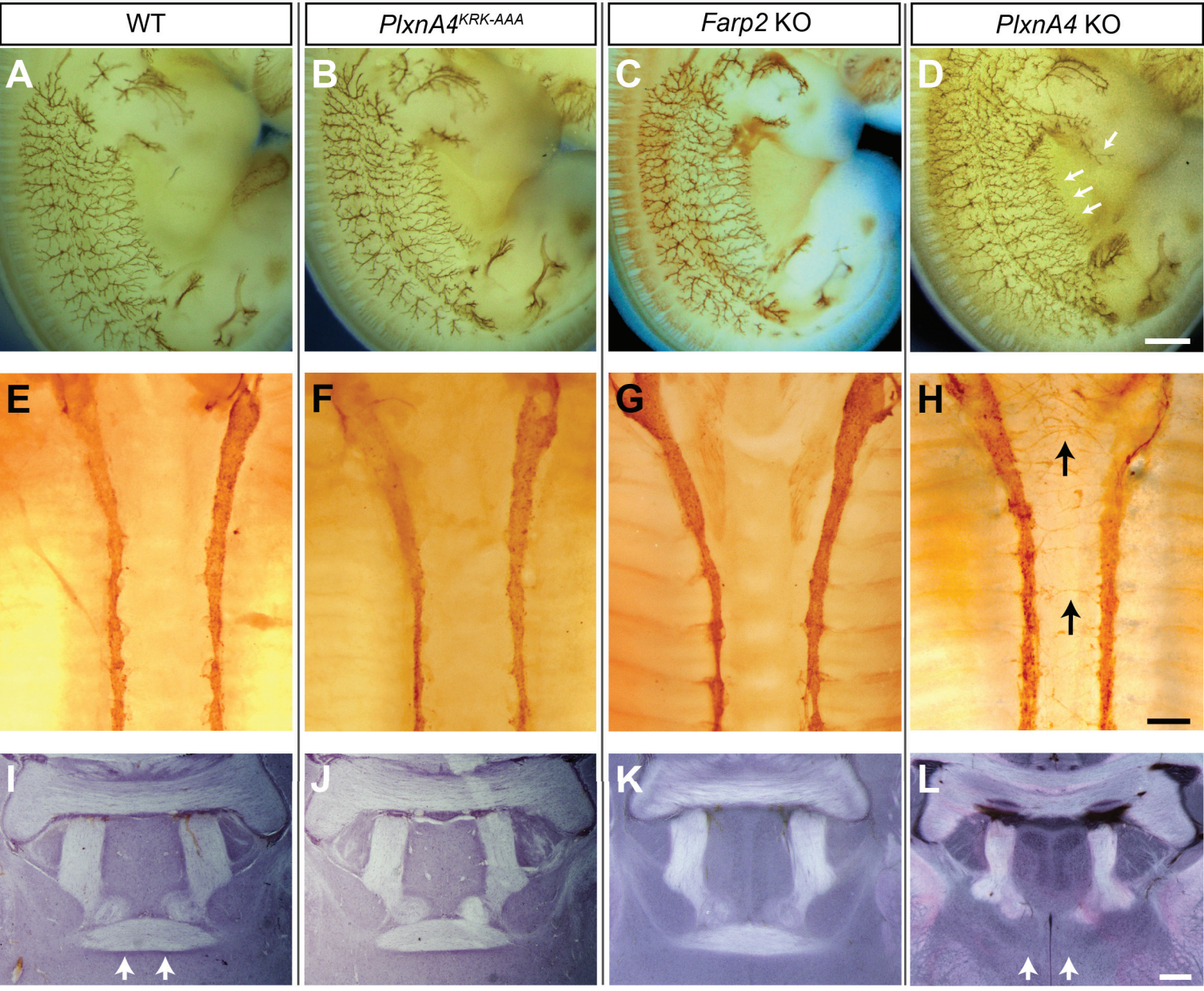

Figure 7

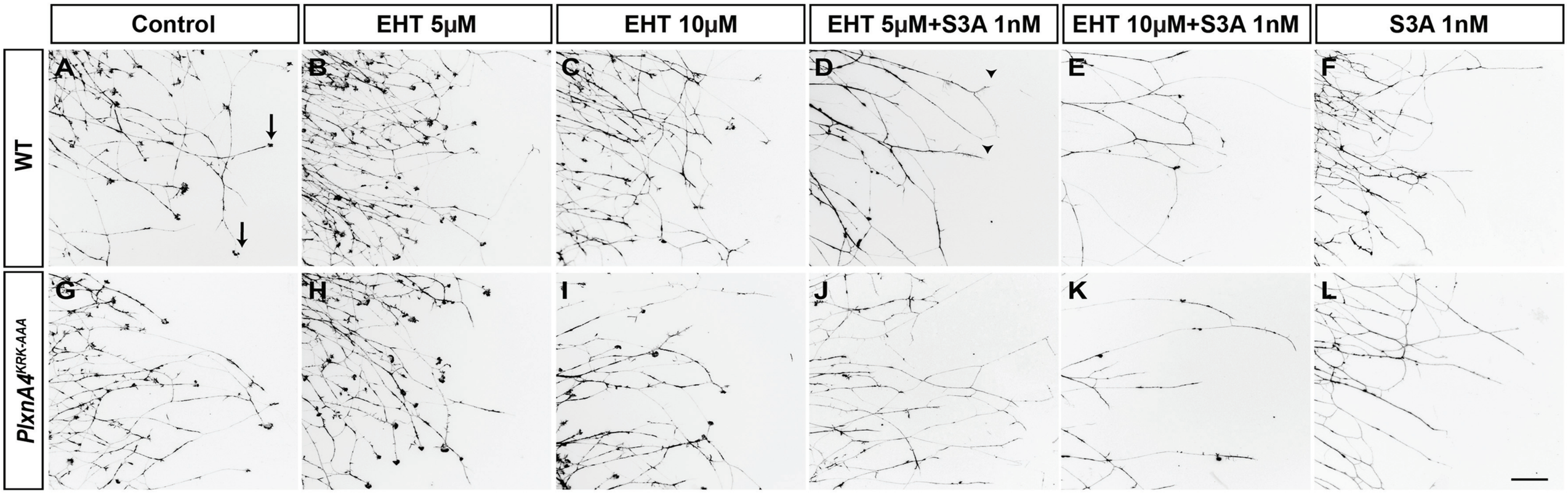
Control
EHT 5μM
EHT 10μM
EHT 5μM+S3A 1nM
EHT 10μM+S3A 1nM
S3A 1nM
WT
PlxnA4KRK-AAA
A
B
C
D
E
F
G
H
I
J
K
L

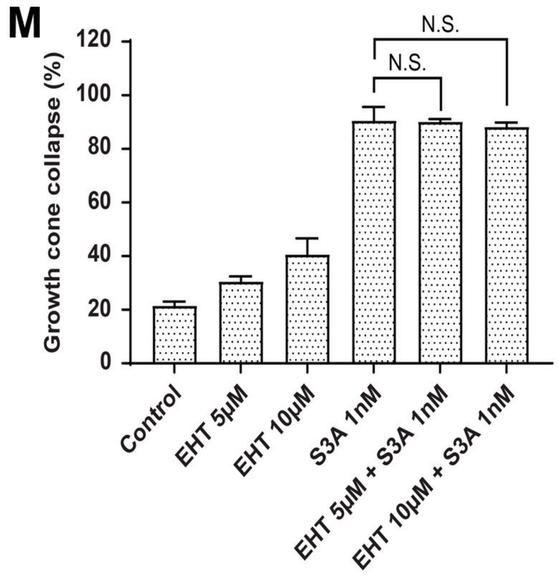
M
Growth cone collapse (%)
120
100
80
60
40
20
0
N.S.
N.S.
Control
EHT 5μM
EHT 10μM
S3A 1nM
EHT 5μM + S3A 1nM
EHT 10μM + S3A 1nM

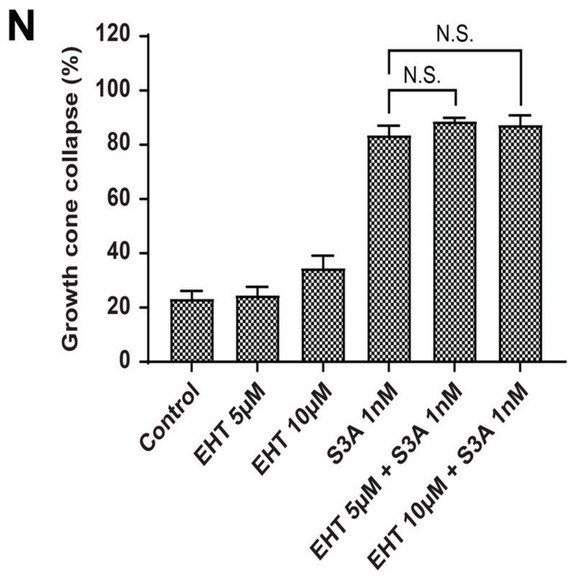
N
Growth cone collapse (%)
120
100
80
60
40
20
0
N.S.
N.S.
Control
EHT 5μM
EHT 10μM
S3A 1nM
EHT 5μM + S3A 1nM
EHT 10μM + S3A 1nM

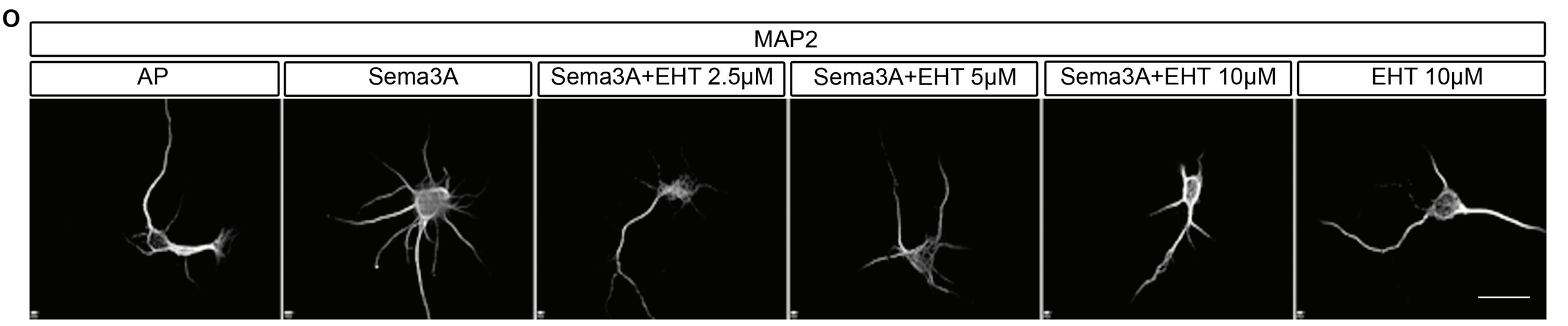
O
MAP2
AP
Sema3A
Sema3A+EHT 2.5μM
Sema3A+EHT 5μM
Sema3A+EHT 10μM
EHT 10μM

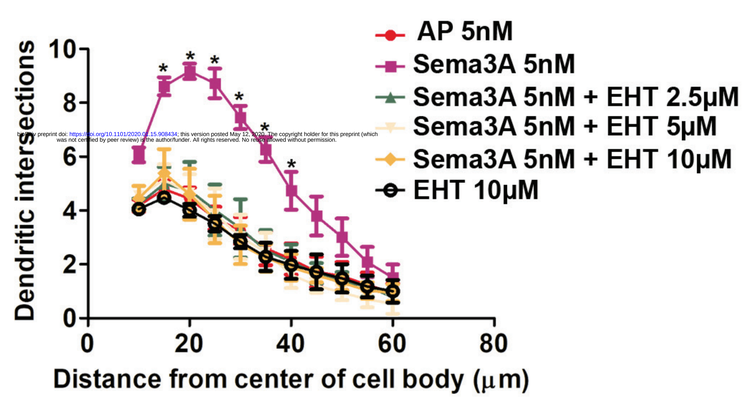
P
Dendritic intersections
10
8
6
4
2
0
0
20
40
60
80
Distance from center of cell body (μm)
AP 5nM
Sema3A 5nM
Sema3A 5nM + EHT 2.5μM
Sema3A 5nM + EHT 5μM
Sema3A 5nM + EHT 10μM
EHT 10μM

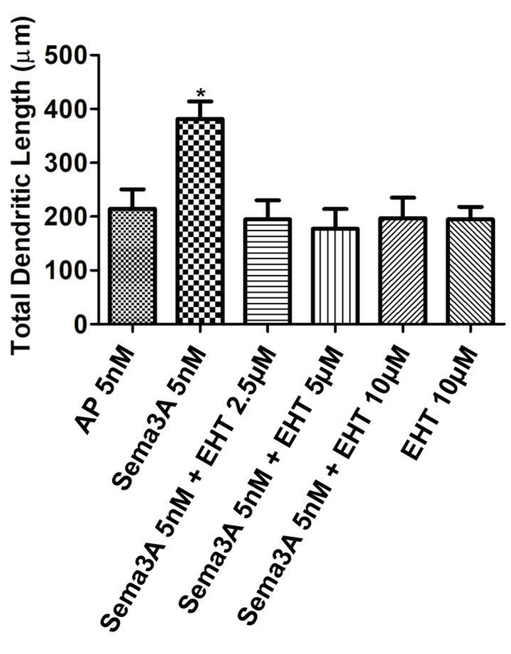
Q
Total Dendritic Length (μm)
500
400
300
200
100
0
AP 5nM
Sema3A 5nM
Sema3A 5nM + EHT 2.5μM
Sema3A 5nM + EHT 5μM
Sema3A 5nM + EHT 10μM
EHT 10μM

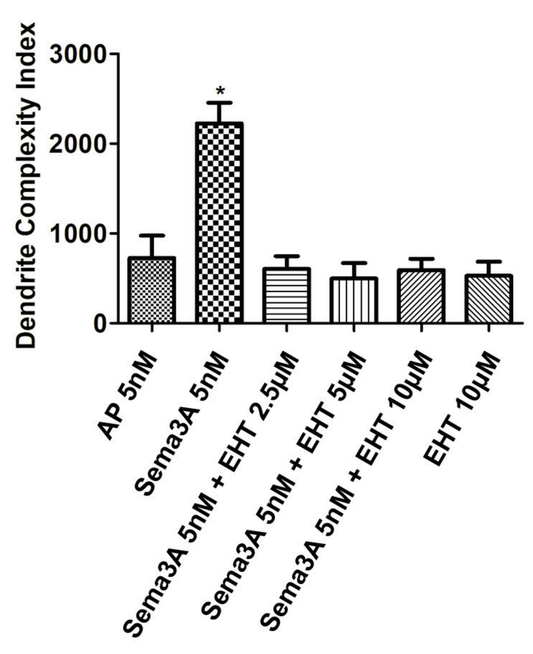
R
Dendrite Complexity Index
3000
2000
1000
0
AP 5nM
Sema3A 5nM
Sema3A 5nM + EHT 2.5μM
Sema3A 5nM + EHT 5μM
Sema3A 5nM + EHT 10μM
EHT 10μM

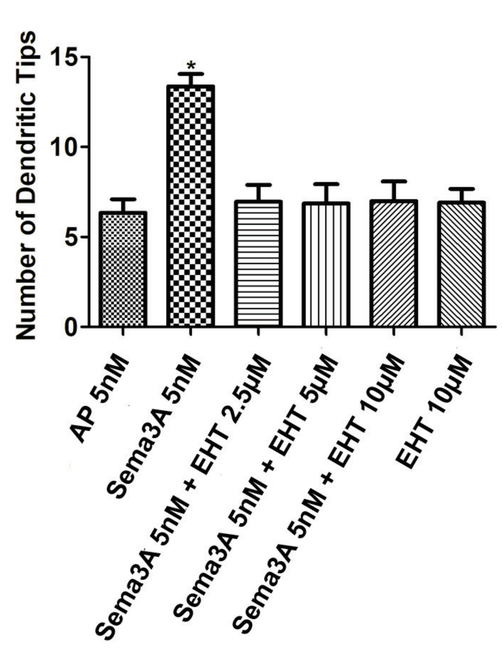
S
Number of Dendritic Tips
15
10
5
0
AP 5nM
Sema3A 5nM
Sema3A 5nM + EHT 2.5μM
Sema3A 5nM + EHT 5μM
Sema3A 5nM + EHT 10μM
EHT 10μM

Figure 8

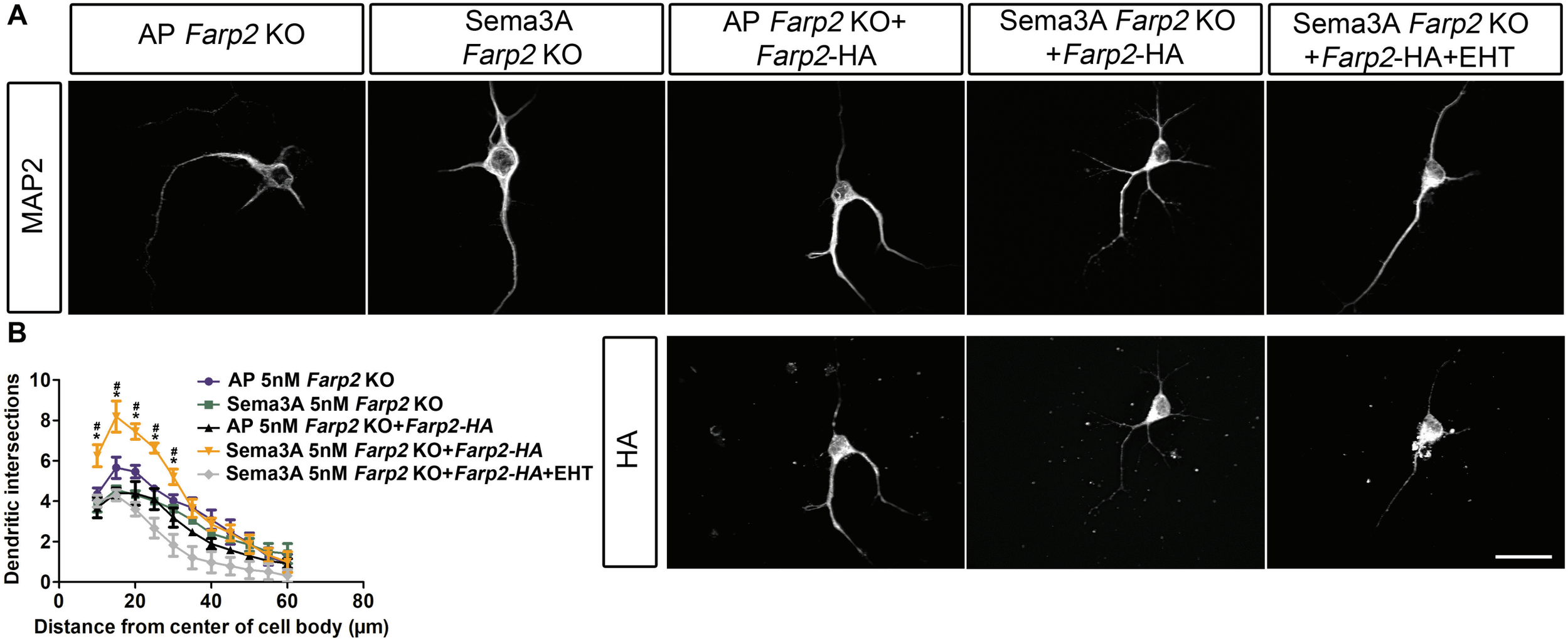
A
AP Farp2 KO
Sema3A Farp2 KO
AP Farp2 KO+ Farp2-HA
Sema3A Farp2 KO +Farp2-HA
Sema3A Farp2 KO +Farp2-HA+EHT
MAP2
HA
B
AP 5nM Farp2 KO
Sema3A 5nM Farp2 KO
AP 5nM Farp2 KO+Farp2-HA
Sema3A 5nM Farp2 KO+Farp2-HA
Sema3A 5nM Farp2 KO+Farp2-HA+EHT
Dendritic intersections
Distance from center of cell body (μm)
0
2
4
6
8
10
0
20
40
60
80

Figure 9

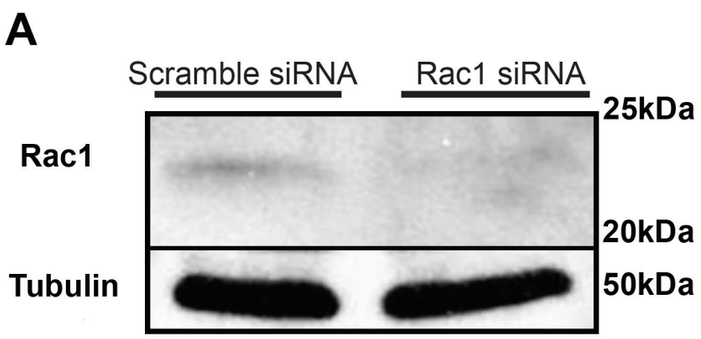

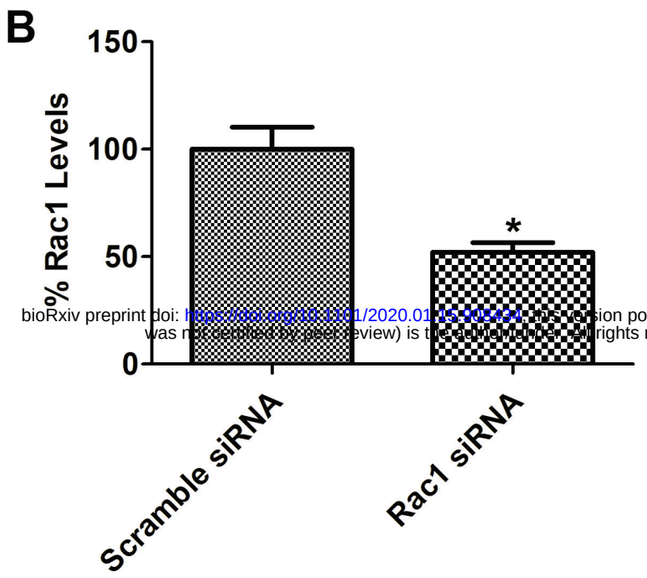

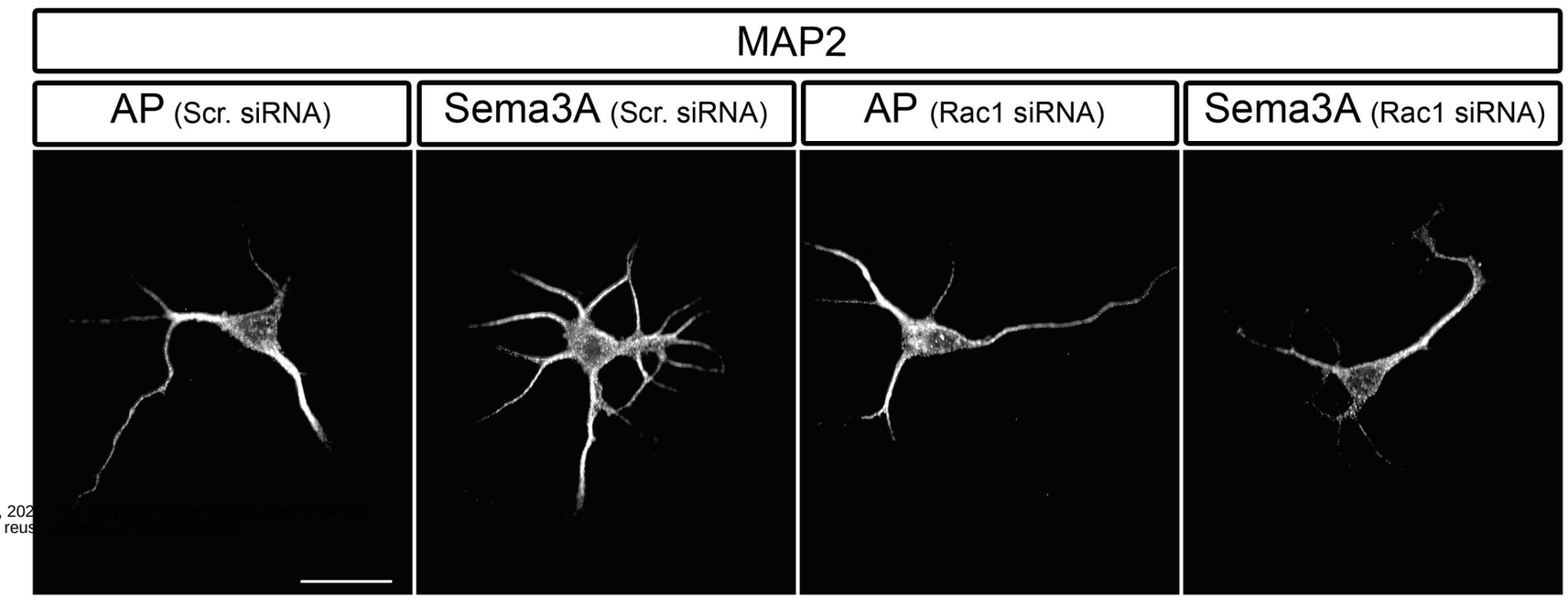

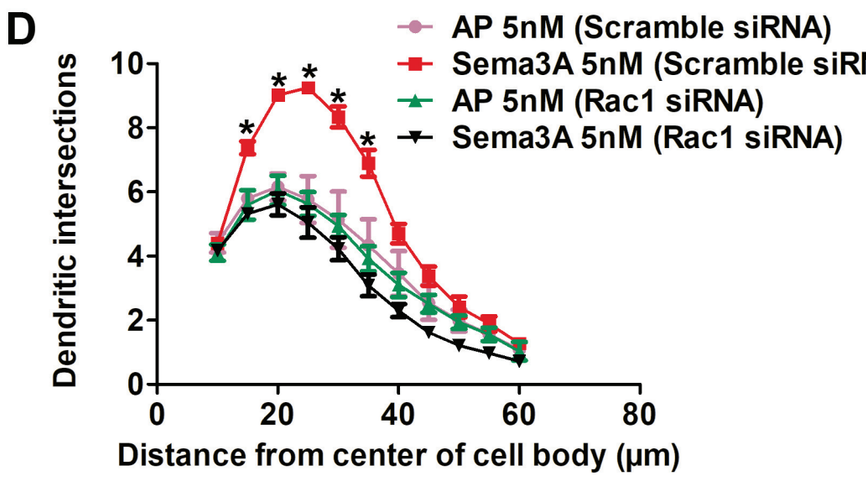

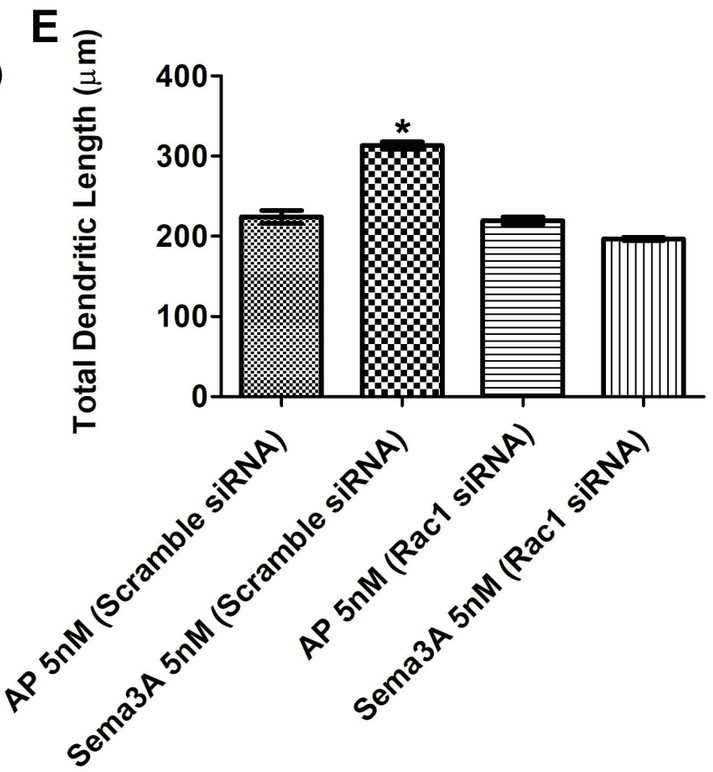

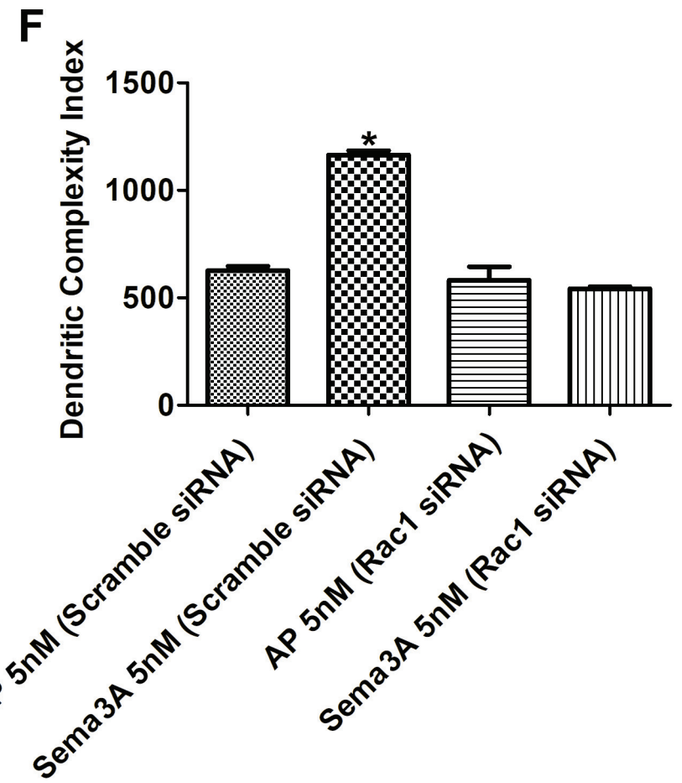

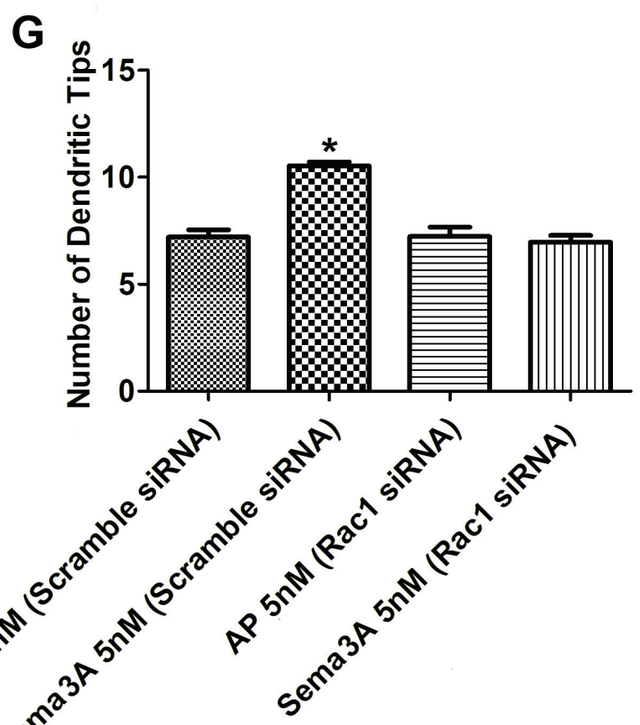

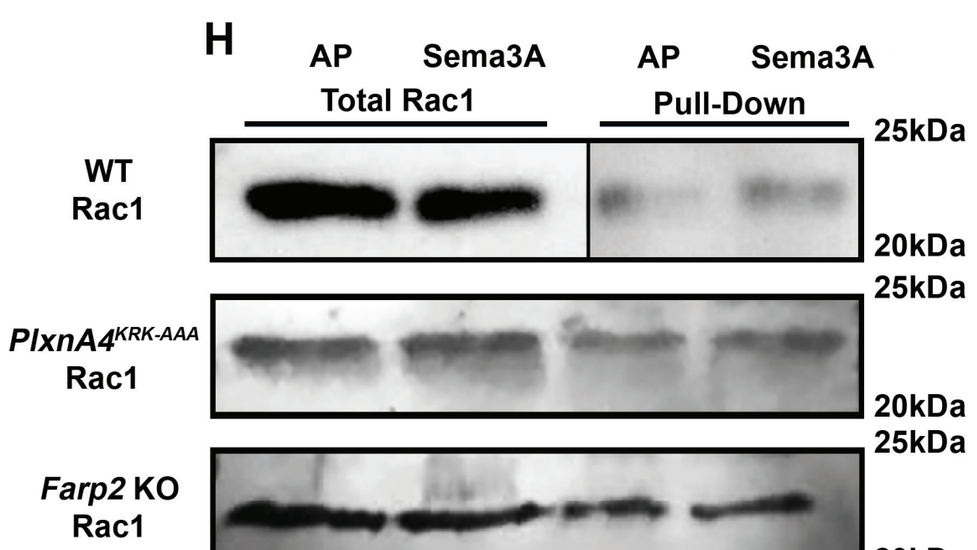

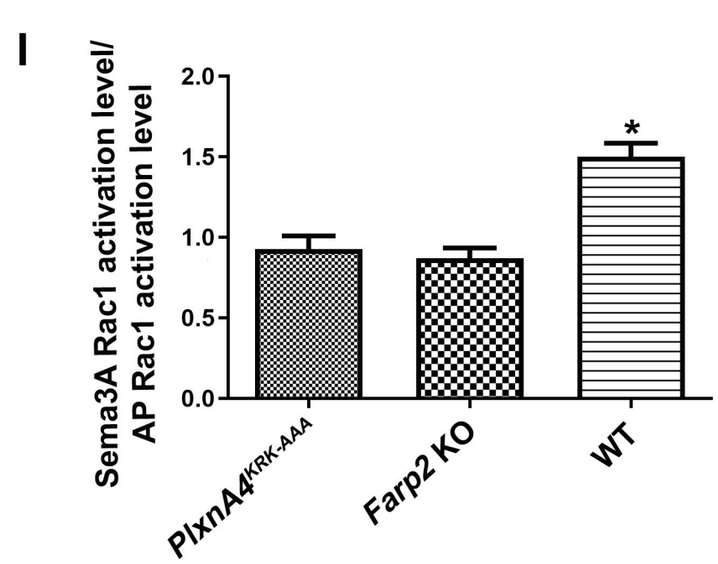

Figure 10

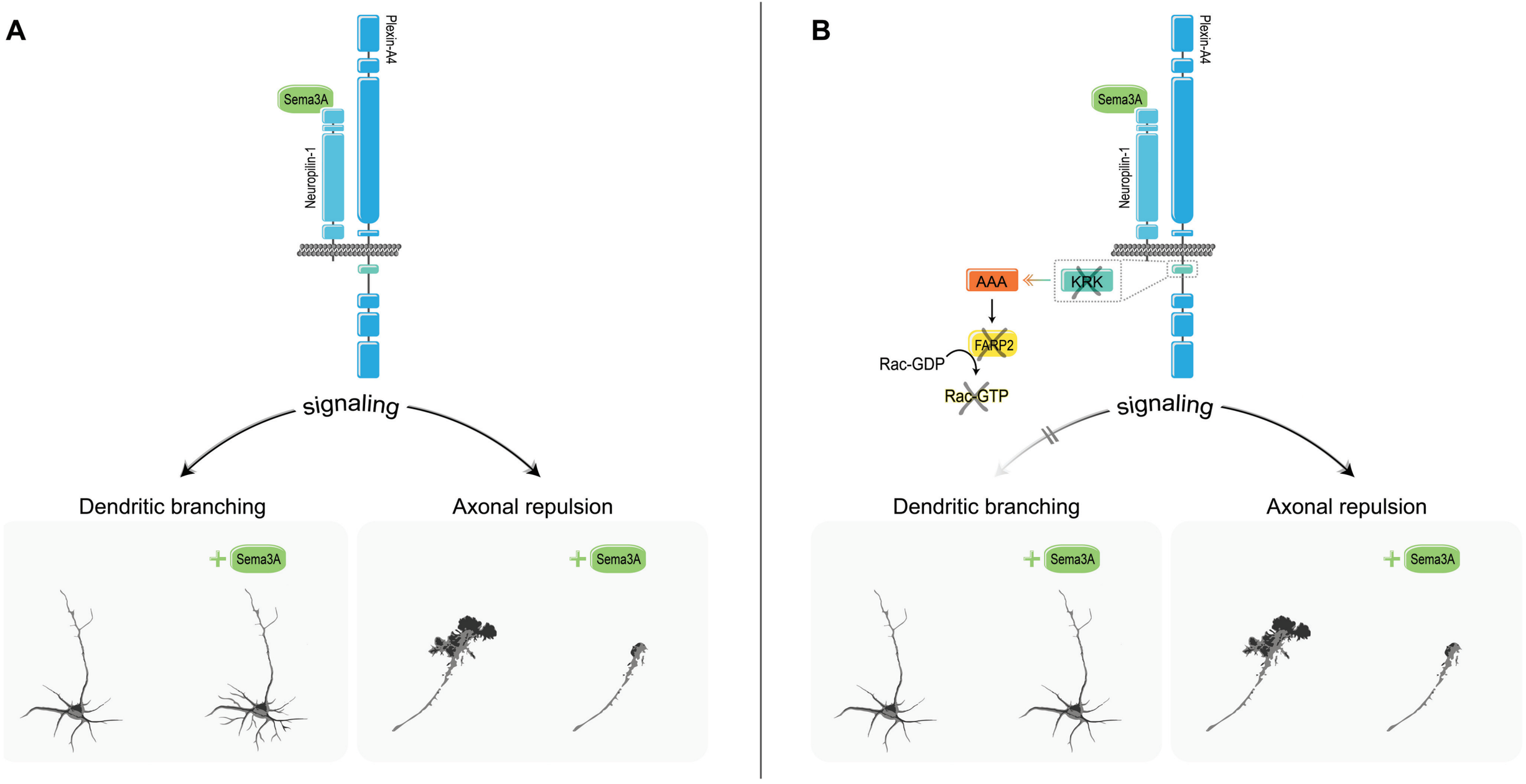
A
Plexin-A4
Sema3A
Neuropilin-1
signaling
Dendritic branching
Axonal repulsion
+ Sema3A
+ Sema3A
B
Plexin-A4
Sema3A
Neuropilin-1
AAA
KRK
FARP2
Rac-GDP
Rac-GTP
signaling
Dendritic branching
Axonal repulsion
+ Sema3A
+ Sema3A